Cataclysmic Variables from Sloan Digital Sky Survey – V. The search for period bouncers continues

K. Inight [1]★ Boris T. Gänsicke [1] A. Schwope,[2] S. F. Anderson,[3] C. Badenes,[4] E. Breedt [5]
V. Chandra [6] B. D. R. Davies,[1] N. P. Gentile Fusillo [7] M. J. Green [1,8] J. J. Hermes [9]
I. Achaica Huamani,[10] H. Hwang,[11] K. Knauff,[2] J. Kurpas,[2,12] K. S. Long,[13] V. Malanushenko,[14]
S. Morrison [15] I. J. Quiroz C.,[10] G. N. Aichele Ramos,[10] A. Roman-Lopes,[16] M.R. Schreiber,[10,17]
A. Standke,[2,12] L. Stütz,[2] J. R. Thorstensen,[18] O. Toloza,[10,17] G. Tovmassian [19] and N. L. Zakamska [20]

[1]*Department of Physics, University of Warwick, Coventry CV4 7AL, UK*
[2]*Leibniz-Institut für Astrophysik Potsdam (AIP), An der Sternwarte 16, D-14482 Potsdam, Germany*
[3]*Astronomy Department, Box 351580, University of Washington, Seattle, WA 98195, USA*
[4]*Department of Physics and Astronomy, University of Pittsburgh Allen Hall, 3941 O'Hara St, Pittsburgh, PA 15260, USA*
[5]*Institute of Astronomy, University of Cambridge, Madingley Road, Cambridge CB3 0HA, UK*
[6]*Center for Astrophysics | Harvard & Smithsonian, 60 Garden St, Cambridge, MA 02138, USA*
[7]*European Southern Observatory, Karl Schwarzschild Straße 2, D-85478 Garching, Germany*
[8]*School of Physics and Astronomy, Tel-Aviv University, Tel-Aviv 6997801, Israel*
[9]*Department of Astronomy & Institute for Astrophysical Research, Boston University, 725 Commonwealth Ave., Boston, MA 02215, USA*
[10]*Departamento de Física, Universidad Técnica Federico Santa María, Avenida España 1680, Valparaíso, Chile*
[11]*Institute for Advanced Study, Princeton, 1 Einstein Drive, NJ 08540, USA*
[12]*Potsdam University, Institute for Physics and Astronomy, Karl-Liebknecht-Straße 24/25, D-14476 Potsdam, Germany*
[13]*Space Telescope Science Institute, 3700 San Martin Drive, Baltimore, MD 21218, USA*
[14]*Apache Point Observatory, PO Box 59, Sunspot, NM 88349, USA*
[15]*Department of Astronomy, University of Illinois at Urbana-Champaign, Urbana, IL 61801, USA*
[16]*Departamento de Astronomía, Universidad La Serena, La Serena, Chile*
[17]*Millennium Nucleus for Planet Formation (NPF), Valparaíso, Chile*
[18]*Department of Physics and Astronomy, Dartmouth College, Hanover NH 03755, USA*
[19]*Universidad Nacional Autónoma de México, Instituto de Astronomía, Aptdo Postal 106, Ensenada 22860, Baja California, México*
[20]*Department of Physics & Astronomy, Johns Hopkins University, Baltimore, MD 21218, USA*

ABSTRACT

SDSS-V is carrying out a dedicated survey for white dwarfs, single, and in binaries, and we report the analysis of the spectroscopy of 118 cataclysmic variables (CVs) and CV candidates obtained during the final plug plate observations of SDSS. We identify eight new CVs, spectroscopically confirm 53 and refute 11 published CV candidates, and we report 21 new or improved orbital periods. The orbital period distribution of the SDSS-V CVs does not clearly exhibit a period gap. In common with previous studies, the distribution shows that spectroscopically identified CVs have a larger proportion of short-period systems compared to samples identified from photometric variability. Remarkably, despite a systematic search, we find very few period bouncers. We estimate the space density of period bouncers to be $\simeq 0.2 \times 10^{-6} \, \mathrm{pc}^{-3}$, i.e. they represent only a few per cent of the total CV population. This suggests that during their final phase of evolution, CVs either destroy the donor, e.g. via a merger, or that they become detached and cease mass transfer.

Key words: stars: evolution – Hertzsprung–Russell and colour–magnitude diagrams – cataclysmic variables.

1 INTRODUCTION

Cataclysmic variables (CVs; see Warner 2003 for a comprehensive overview) are interacting binaries in which a white dwarf is accreting from a low-mass companion. They are a key population for testing and developing our understanding of close binary evolution and interaction (Belloni & Schreiber 2023). The shortest-period systems

are among the verification sources for the space-based gravitational wave mission LISA (Kupfer et al. 2018), and they provide ideal laboratories for the study of accretion discs (Hameury 2020) and accretion onto magnetic stars (Cropper 1990; Ferrario, de Martino & Gänsicke 2015).

However, because of their wide range of observational properties, the known population of CVs remains subject to severe selection biases (Gänsicke 2005). Even the census of CVs within 150 pc is currently only $\approx$77 per cent complete; the undiscovered CVs will almost entirely be systems that show little optical variability (Pala

★ E-mail: keith.inight@gmail.com

et al. 2020) such as low-accretion rate WZ Sge systems (Tampo et al. 2020) and high-accretion rate nova-like variables (Inight et al. 2022).

The Sloan Digital Sky Survey (SDSS) (York et al. 2000) has proven to be an important tool for identifying CVs spectroscopically (Szkody et al. 2002, 2003, 2004, 2005, 2006, 2007, 2009, 2011), with the total number of CVs observed by SDSS standing at 507 (Inight et al. 2023). Follow-up studies of individual SDSS CVs led to a large number of notable individual results, including the identification of brown-dwarf donors (Schmidt et al. 2005c; Littlefair et al. 2006a), the identification of low-mass transfer magnetic CVs (Schmidt et al. 2005b, 2007), the first eclipsing AM CVn (Anderson et al. 2005), nuclear evolved CVs (Littlefair et al. 2006b; Rebassa-Mansergas et al. 2014), pulsating white dwarfs (Gänsicke et al. 2006; Mukadam et al. 2007; Pavlenko et al. 2014), and a halo CV (Uthas et al. 2011), as well as the detection of spiral shocks (Aviles et al. 2010; Pala et al. 2019). The SDSS spectroscopy led, in particular, to the discovery of a large number of CVs with no history of outbursts; analysis of these systems confirmed the long-standing prediction of a pile-up of CVs near the minimum orbital period of about 80 min (Gänsicke et al. 2009).

During the commissioning of SDSS, Raymond et al. (2003) developed a targeting strategy for CVs in *ugriz* colour space, which, however, proved to be more effective in identifying detached white dwarf plus M-dwarf binaries. As remarkable as the impact of SDSS has been on the research of CVs, most of the SDSS CVs were observed serendipitously in a much larger pool of objects targeted for spectroscopy for a wide range of reasons, e.g. as quasar candidates or blue excess objects (Strauss et al. 2002) or because of their variability (Morganson et al. 2015).

SDSS has now entered its fifth phase (SDSS-V, Kollmeier et al. 2017), which will extend multi-object spectroscopy across the entire sky by operating robotic fibre positioners on the 2.5 m SDSS telescope at Apache Point Observatory (APO) and at the 2.5 m Dupont telescope at Las Campanas Observatory. SDSS-V differs from its predecessors in which it contains a program to deliberately target white dwarfs and CVs. Although most of SDSS-V will be carried out with robotic positioners, the first eight months of SDSS-V observations at APO followed the approach using fibres positioned in the focal plane with drilled plates (Blanton et al. 2003) to feed a spectrograph, as used in the earlier phases of SDSS.

We report here on the 118 CVs observed in the first eight months of SDSS-V as part of the dedicated white dwarf binary targeting strategy. We describe the identification of new CVs, the spectral confirmation of candidate CVs, and new observations of previously known CVs. We report new orbital periods for 21 of these CVs obtained by combining radial velocity data from SDSS with light curves from the Zwicky Transient Facility (ZTF; Bellm et al. 2019) and other follow-up observations. The remainder of this manuscript is organized as follows. We describe the target strategy in Section 2 and our observations in Section 3. We describe how we analyse and classify the spectra and light curves in Section 4, report our results in Section 5, and discuss our findings in Section 6. Finally, we summarize our results in Section 7. A complete table of information about the observed systems is included in the appendix.

2 TARGET SELECTION

Whereas the previous generations of the SDSS surveys were prolific in identifying new CVs, the vast majority of these systems were observed serendipitously, many of them because they overlap in colour space with quasars (see for example Richards et al. 2002; Gänsicke et al. 2009). SDSS I to IV preceded *Gaia* (Gaia Collaboration 2018), therefore parallaxes, and hence absolute magnitudes

were not available, and the only dedicated target selection for CVs relied on rather crude colour-colour cuts, which were in fact more successful in identifying detached white dwarf plus M-dwarf binaries (Raymond et al. 2003). The CVs within SDSS I to IV were identified by visual inspection of the SDSS spectroscopy, sometimes aided by various techniques filtering the entire SDSS data set into shortlists of candidate objects to be inspected (e.g. Szkody et al. 2002, 2003, 2004, 2005, 2006; Carter et al. 2014; Gentile Fusillo, Gänsicke & Greiss 2015; Kepler et al. 2019, 2021; Inight et al. 2023).

SDSS-V provided the first opportunity to define dedicated target selections aimed at white dwarfs and CVs that made use of the *Gaia* astrometry. These target selections are defined using 'cartons', most of which use a set of algorithmic rules, filtering large catalogues of objects, to produce the target lists for SDSS-V (see table 2 in Almeida et al. 2023 and the description of the compact binary and white dwarf cartons). We defined eight cartons using a range of criteria to target white dwarfs, both single and in binaries: `mwm_wd_core` is based on the *Gaia* white dwarf candidate catalogue of Gentile Fusillo et al. (2019), whereas `mwm_cb_gaiagalex`, `mwm_cb_uvex1`, `mwm_cb_uvex2`, `mwm_cb_uvex3`, `mwm_cb_uvex4`, and `mwm_cb_uvex5` leverage the fact that both single white dwarfs and those in binaries (detached and CVs) have an ultraviolet excess. These ultraviolet-excess cartons are based on cross-matching *Gaia* with ultraviolet surveys, including *GALEX* (Morrissey et al. 2007), the ultraviolet observations obtained by the Optical Monitor of *XMM-Newton* (Mason et al. 2001; Page et al. 2012), and the UVOT instrument onboard *SWIFT* (Gehrels et al. 2004; Roming et al. 2005). These ultraviolet-excess cartons contain a substantial proportion of, but not all, the CVs in the observable SDSS-V footprint. Finally, we defined a carton, `mwm_cb_cvcandidates`, that contains a collection of published CVs and CV candidates (potential CVs that have typically been identified by an outburst and need confirmation with a spectrum). Full details of the target selection rules will be provided in a forthcoming publication. These eight cartons were then assigned priorities for the SDSS-V observations that were above most of the other stellar and extragalactic cartons, ensuring a high completeness of the spectroscopic follow-up. One important fact to bear in mind in the analysis of the SDSS-V results is that a given target can be selected by multiple cartons.

When referring to individual systems, we abbreviate their SDSS designations to four digits in each of RA and Dec., e.g. SDSS J062429.71+002105.8, is referred to as J0624 + 0021. The full designations are listed in Table A1.

3 OBSERVATIONS

3.1 SDSS spectroscopy

The SDSS BOSS spectrograph (Dawson et al. 2013; Smee et al. 2013) covers the range $3600 - 10\,400$ Å. The data analysed here were processed with v6_1_0 of the SDSS-V pipeline (Almeida et al. 2023), which performed sky subtraction together with flux and wavelength calibration of each exposure. Based upon our analysis, the SDSS-V spectroscopy can be used to measure radial velocities from narrow spectral lines with an accuracy of up 20 km s^{-1}. SDSS-V differs from the preceding surveys in that it expanded the coverage to include the Galactic disc, which introduces new challenges; in particular, the reddening effect of interstellar dust has impacted the flux calibration of a number of spectra.

SDSS-V spectroscopy of the cartons described in Section 2 was carried out on 236 individual plates, where each plate covers $\simeq 7\,\mathrm{deg}^2$ of the sky. Sixteen pairs of plates had identical plate centre

Table 1. Target cartons observed by SDSS-V and used for the analysis in this paper showing the completeness. The numbers observed per carton refer to the 236 plates observed as part of SDSS-V in which these cartons were implemented in the observing strategy. Many targets are present in multiple cartons.

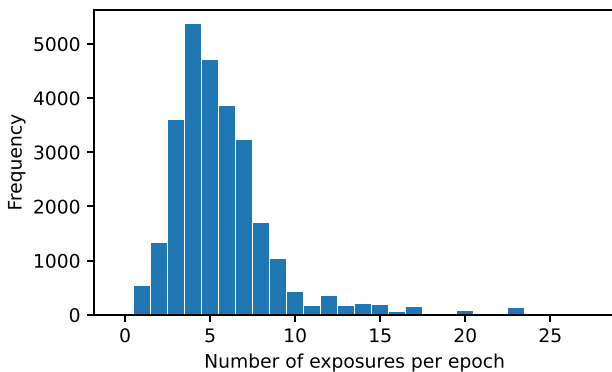| Carton	Targets	Number observed	Per cent complete	CVs found
mwm_cb_gaiagalex	7773	4050	52	26
mwm_cb_uvex1	3281	2488	76	27
mwm_cb_uvex2	8040	5802	72	44
mwm_cb_uvex3	29	24	83	0
mwm_cb_uvex4	179	144	80	2
mwm_cb_uvex5	282	27	10	0
mwm_wd	6229	5781	93	18
mwm_cb_cvcandidates	141	124	88	101

Figure 1. Distribution of the number of 900 s exposures used to form each of the 27 191 co-added spectra. The exposures were often contiguous but always obtained within a 2–3 d epoch. When an object was observed in more than one epoch, a separate co-added spectrum was produced for each epoch.

coordinates. The number of targets per carton, observed targets per carton, spectroscopic completeness, and the number of CVs identified per carton are reported in Table 1. The exposure time for each plate observation was 900 s. A number of exposures were taken, which were often, but not always, contiguous. The pipeline collects all the exposures of a given plate within 2 − 3 d (a 'plate-epoch' hereafter referred to as an epoch) and co-adds the individual spectra for each target (see Fig. 1). We use the co-added spectrum for our spectral classification identification as it will have a higher signal-to-noise ratio (SNR) than the individual 900 s spectra. We use the individual spectra to probe for variations in radial velocity. The plate observations of SDSS-V collected 27 191 co-added spectra of 11 384 individual targets that fall within our cartons (many plates were observed at different epochs, separated by weeks to months, resulting in multiple co-added spectra of a substantial number of targets).

The CV sample presented in this paper is therefore not complete within the SDSS-V plate program and is limited to the systems targeted in the cartons described above – additional CVs may emerge from the extragalactic programs, although these are most likely to be too faint to have a *Gaia* counterpart.

3.2 Photometric survey data

We retrieved archival light curves from the Catalina Real-Time Transient Survey (CRTS; Djorgovski et al. 2011), ZTF (Bellm et al. 2019), and the Transiting Exoplanet Survey Satellite (*TESS*, Ricker et al. 2015). We reviewed these primarily for historical outbursts.

Table 2. The journal of the Liverpool Telescope observations.

Date	UTC (start)	N (obs)	Duration (minutes)
J0624 + 0021			
2021 December 29	22:27:40	120	218
2022 January 05	22:40:53	90	162
J1740 + 0258			
2022 June 03	23:09:51	180	325
2022 June 20	22:41:14	200	262

The ZTF and *TESS* light curves are shown alongside the spectra in Figs 1–13 in the supplementary material.

3.3 Follow-up observations

3.3.1 Photometry

We obtained follow-up photometry using the 2 m Liverpool Telescope (LT, Steele et al. 2004, see Table 2 for details) of two particularly interesting CVs: J0624 + 0021, which is located in the period gap (Section B9) and J1740 + 0258, which exhibits unusual state changes (Section B33). Both systems were identified as potentially eclipsing systems from their SDSS spectra where the higher Balmer lines exhibit deep central absorption dips that go down to, or even below the continuum. Both targets were observed twice. The length of the initial observation was chosen to exceed the likely orbital period so that at least one eclipse would be observed. In both cases, the first observation covered two eclipses, from which we estimated the orbital period, and then scheduled a second observation a few days later to provide a more accurate period measurement. Each LT observation consisted of a sequence of 90 s exposures with the IO:O imager using a Bessel-*V* filter. The standard LT pipeline was then used to provide bias subtraction and flat fielding. Differential photometry was obtained with the SEXTRACTOR package (Bertin & Arnouts 1996), using *Gaia* EDR3 3 120 280 993 084 993 792 as comparison star for J0624 + 0021 and *Gaia* EDR3 4 376 322 089 783 941 120 for J1740 + 0258.

3.3.2 Spectroscopy

Prior to SDSS-V, one of the authors (JRT) obtained time-resolved spectroscopy using the 2.4 m Hiltner telescope of the MDM observatory at Kitt Peak (see Thorstensen 2020 for more details on the instrument and data reduction techniques) of the CV candidate J0418 + 5107 (NS Per) because it appeared to be suitable for a radial-velocity based period determination. We present here the so far unpublished results of these observations (Section C5).

4 ANALYSIS

4.1 Classification

Classification consists of first identifying the CVs among the 27 191 SDSS-V co-added spectra and then determining the sub-type of each CV.

4.1.1 CV identification

We initially scanned each spectrum by eye for indications of a CV nature – typically the presence of emission lines but see Inight et al. (2023) for a full description of the spectral characteristics of CVs. Although in theory this process could be automated, there was a risk

that some important exotic object could be missed (such as nova-like variables and dwarf novae observed during outburst, which have disc-dominated spectra with, in some cases, very weak absorption lines). In addition, some plates near the Galactic plane that were subject to substantial amounts of reddening had very poor flux calibrations, and CV spectra obtained on those plates would very likely have been missed in any automated search.

The list of CVs obtained from this visual inspection was then compared with CV catalogues (Ritter & Kolb 2003; Watson, Henden & Price 2006) to identify previously known CVs and then subjected to more detailed scrutiny using the available archival information (light curves, astrometric, and photometric data). New CVs identified in SDSS-V and systems where the SDSS-V spectra refute previously published CV classifications are discussed in Section 5, detailed notes on previously known CVs where the SDSS-V spectra confirms their classification are given in Appendix B, and Appendix C includes notes on a selection of well known CVs where SDSS-V has revealed new information.

Several CVs were observed at different epochs by SDSS-V and the resulting co-added spectra were compared and merged where appropriate. As part of this process, we found four CVs (J0528 − 0333, J0808+3550, J0926+0345, and J1830 + 2655) that were observed in both outburst and quiescence and these are shown separately in Fig. 13 in the supplementary material.

The final list of CVs (Table A1) was then subjected to a rigorous search of the literature to find references both for the initial claim of a CV nature, the first published spectrum, and the most accurate measurement of the orbital period.

4.1.2 CV sub-types

CVs are categorized into a number of sub-types based on their observed characteristics, with the sub-types often being named after a prototype CV that exemplifies particular characteristics. In this paper, we have used the classifications from the literature where available, making additions and corrections where appropriate.

In the companion paper on CVs observed by in SDSS I to IV (Inight et al. 2023), we describe the taxonomy of CVs and summarize the salient stages of CV evolution. The following is a highly simplified overview:

Non-magnetic CVs ($B \lesssim 1\,\mathrm{MG}$) that exhibit disc outbursts are dwarf novae, those with steady hot discs are nova-like variables. Dwarf novae are further sub-classified into SU UMa CVs (typically short-period, $P_{orb} \lesssim 3\,h$, that have relatively frequent outbursts, interspersed by longer and brighter superoutbursts), ER UMa CVs (systems with very short superoutburst recurrence times), WZ Sge CVs (which only have rare superoutbursts), U Gem CVs (typically long-period, $P_{orb} \gtrsim 3\,h$, dwarf novae that do not show superoutbursts), and Z Cam CVs (that switch between outburst states and 'standstill' periods of constant brightness). CVs with highly magnetic white dwarfs (MCVs) consist of polars (which typically have $B \gtrsim 10\,\mathrm{MG}$ and the white dwarf spin period synchronized with the orbital period, $P_{spin} = P_{orb}$) and intermediate polars (IPs, with $10 \gtrsim B \gtrsim 1\,\mathrm{MG}$, and $P_{spin} < P_{orb}$). Finally, AM CVn CVs are ultra-short period ($P_{orb} \lesssim 60\,\mathrm{min}$) hydrogen-deficient CVs.

We classified all SDSS-V CVs by considering all available data. This includes not only the spectrum but also CRTS, ZTF, and *TESS* light curves, spectral energy distributions (SED) based on the available broad-band photometry, Hertzsprung–Russell (HR) diagrams based on the *Gaia* astrometry and photometry, and Pan-STARRS images. CVs for which we were unable to determine a sub-type are simply classified 'CV'.

4.2 Orbital periods

We use a combination of spectroscopically derived radial velocities (SDSS and the MDM Observatory) and photometric light curves (ZTF) to estimate orbital periods.

4.2.1 Radial velocities from SDSS-V

The measurement of radial velocities from the Doppler shifts of emission lines and their variation over an orbital period have a long history of determining the period of a CV (Merrill 1923). The emission lines are assumed to arise from the accretion disc around the white dwarf and to track the orbit of the white dwarf around the centre of gravity of the CV. The observed velocity is smaller than the Keplerian velocity of the white dwarf, $v_{obs} = \sin i \times v_{wd}$ with i, the inclination of the binary, which implies that orbital periods for low inclination systems may be difficult to impossible to measure.

The spectroscopy of the CVs in SDSS-V consists of one or more epochs in each of which multiple 900 s exposures were obtained (see Fig. 1). In contrast to the co-added identification spectra shown in Section 5 and the supplementary material, many of the individual 900 s exposures have low SNR, and some of them are affected with cosmic ray artefacts that had to be manually identified and removed. In order to measure radial velocities from these individual spectra, we developed a two-step procedure simultaneously fitting two Gaussians (to model double-peaked emission lines) to each of the first four Balmer lines, Hα to Hδ, using the same radial velocity (Fig. 2). The LMFIT package provides a straightforward way to achieve this in PYTHON. Prior to fitting, we normalized the continuum around each of the four Balmer lines in each exposure to unity by means of a first-order polynomial fit.

In the first step, we notice that a Gaussian has three free parameters – central wavelength (μ), width (σ), and amplitude (A):

$$f(\lambda; A, \mu, \sigma) = \frac{A}{\sigma \sqrt{2\pi}} \exp\left(-\frac{1}{2}\left(\frac{\lambda - \mu}{\sigma}\right)^2\right) \quad (1)$$

For this step, we created an LMFIT (Newville et al. 2016) model of the form:

$$C + \sum_{i \in \{\alpha, \beta, \gamma, \delta\}} \Big(f\left(\lambda; A_{i,1}, \lambda_i - s/2, \sigma_{i,1}\right) + f\left(\lambda; A_{i,2}, \lambda_i + s/2, \sigma_{i,2}\right) \Big) \quad (2)$$

where

$$\lambda_i = \mu_i + \sqrt{\frac{1 - v/c}{1 + v/c}} \quad (3)$$

Here μ_i is the central wavelength of the i(th) Balmer line, s is the difference in wavelength between the centres of the two Gaussians, and v is the radial velocity causing the Doppler shift; C is a constant. This model is fitted to each exposure, in turn allowing all the free parameters to vary. In a few cases where the spectrum shows a steep Balmer decrement and the higher order lines are not visible, we limit the process to Hα and Hβ.

For the second step, a template model of the form (2) is formed by averaging the values of each of the free parameters derived in the first step over the exposures. The template model is then fitted to each exposure with only v being allowed to vary.

With a set of measured radial velocities in hand, the next step is to estimate the period. This is inherently difficult because the data set is sparse, and so we use a two (three) pronged approach, based on
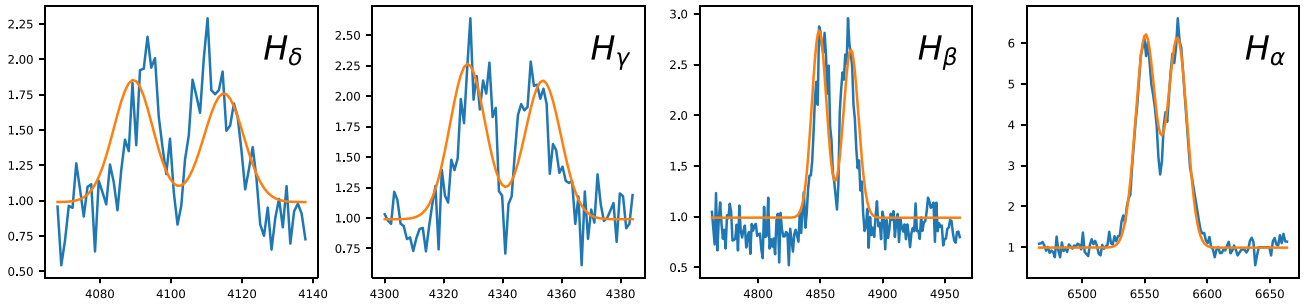
Figure 2. Example of extracting radial velocities by fitting a template of four double-Gaussian profiles (orange) to an individual 900 s spectrum of J0633 + 0303 (blue). The observed spectrum and the template are both normalized to unity individually for each Balmer line. The radial velocity of the CV is measured by fitting all four Balmer lines simultaneously with a single free parameter for the velocity.

sine fits to the radial velocities, the use of the PYTHON package called THE JOKER (Price-Whelan et al. 2017) and ZTF periodograms where available. We consider a period trustworthy where the approaches give consistent results. To fit a sine wave, we use LMFIT to fit an equation of the form:

$$g(t; K, P, \phi, v_{sys}) = K \sin\left(\frac{2\pi t}{P} + \phi\right) + v_{sys} \qquad (4)$$

where K, P, and ϕ are the amplitude, period, and phase of the radial velocity variation, and v_{sys} is the systemic velocity. Unfortunately, when seeking the optimal values of the four free variables, LMFIT is very sensitive to the initial values with which it is seeded and will select a solution giving a local minimum for χ^2, which will not always be the correct one. To address this problem, we used an existing published value or a photometric estimate (e.g. from ZTF) where available to seed the process.

We also used THE JOKER to help identify the correct alias. THE JOKER makes prior assumptions about the distribution of six parameters – namely orbital period, eccentricity,[1] pericentre phase and argument, velocity semi-amplitude, and the barycentre velocity. These distributions are used to create a large set of samples, which are then compared with the observed data to obtain posterior distributions and hence the most likely alias.

The accuracy of a period derived from radial velocities depends heavily upon the SNR of the data, the number of exposures, and the number of epochs.

4.2.2 Light curves from ZTF

The plate survey of SDSS-V and ZTF have similar coverage in the northern sky, so most of our CVs and CV candidates have ZTF data. ZTF saw first light in November 2017 and is designed to survey the sky every $\simeq$3 d, although some areas are observed more frequently in the search for extragalactic transients (Bellm et al. 2019). The number of ZTF photometric data points varies with the location on the sky with median values of 260 and 482 for the *g* and *r*-band, respectively. Some objects additionally have a few nights of high cadence (with images obtained typically every few minutes for several hours) observations, which are particularly useful for measuring orbital periods. Before searching for periodic behaviour, it is necessary to remove outbursts and also remove any long-term trends (see Fig. 3). We defined a threshold for each object to clip outbursts and used a

---

[1]For the purpose of our analysis, we assume that the orbit is circular and that any small ellipticity can be ignored.
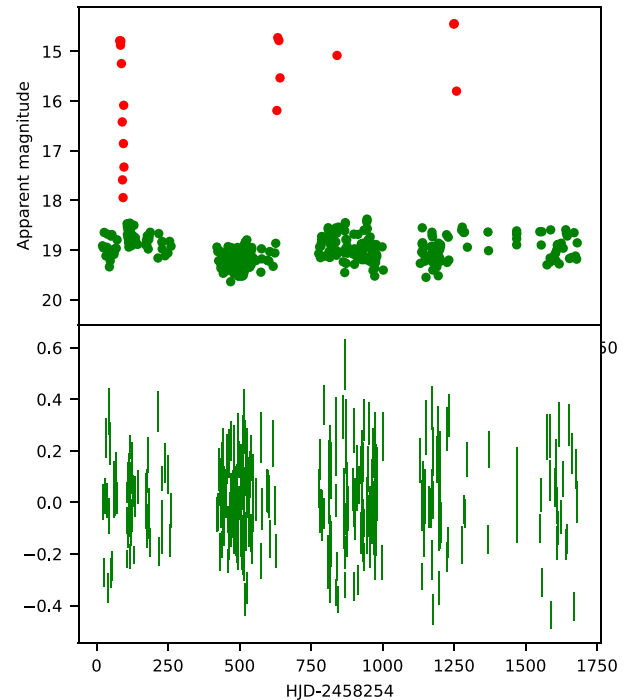
Figure 3. Top panel: ZTF light curve of J0038 + 2509 showing the outbursts in red. Bottom panel: The same light curve, clipped to remove the outbursts and with long-term trends removed.

polynomial filter to remove trends. The filter spans a longer time than any potential orbital period. We then computed a periodogram (see Fig. 4) using two techniques: a Fourier analysis (Deeming 1975) and the 'Multi-harmonic Analysis of Variance' (AOV) algorithm (Schwarzenberg-Czerny 1989). The Fourier analysis works well for sinusoidal light curves whilst the AOV is superior for light curves with more complex structures, e.g. cyclotron beaming or eclipses. For the 66 systems studied here that had no period measurement, ZTF periodograms provide a unique reliable period in only eight cases (typically where there is high cadence data), but they also help to identify the correct alias from periods derived from radial velocities. Depending on the physical origin of the photometric modulation, the strongest signal in the ZTF periodograms could be equal to the orbital period (e.g. for eclipsing CVs) or half the orbital period (e.g. for systems where the donor contributes significant amounts of light,

Figure 4. Top panel: The ZTF power spectrum of J0635+0303. The strongest signal is likely to be the orbital period and was used to seed the analysis of the radial velocity variations. Bottom panel: The ZTF power spectrum of J0038 + 2509, showing the strongest signal at 2.26 h, and a slightly weaker signal at the second harmonic. The strongest signal is consistent with the superhump period of 2.33 h found by Kato et al. (2012) and is therefore the orbital period.

resulting in ellipsoidal modulation, or cyclotron beaming in a polar), so care has to be taken in the interpretation of photometric periods.

4.2.3 Eclipses from the Liverpool Telescope

We measured the eclipse timings of J0624+0021 and J1740+0258 from the LT light curves (Figs B1 and B3) by fitting a Gaussian to the eclipse profiles. In each case, two eclipses were covered by the initial LT observation, and accurate periods were then determined from this estimate combined with the second sets of LT data, and the periodogram calculated from the ZTF data.
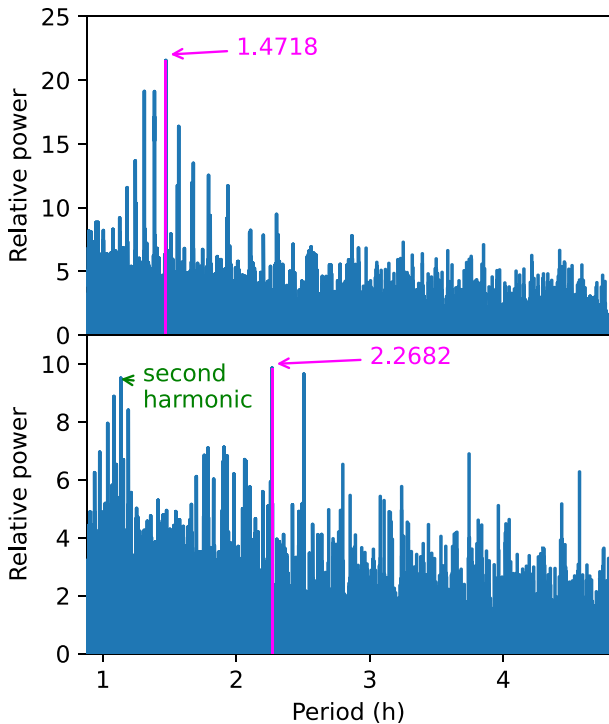
5 RESULTS

Details of all 118 CVs observed in SDSS-V are listed in Table A1. We identified eight new CVs, obtained the first spectrum for 45 previously known CVs and CV candidates, and disproved the published CV classification of eleven systems. The co-added spectra and light curves for the eight new CVs are shown in Fig. 5, and the properties of these systems are discussed in Section 5.1. The spectra and light curves of 110 previously known CVs and candidate CVs are shown in Figs 1–13 in the supplementary material and any new information on these systems is discussed in Appendices B and C. The spectra and light curves of the eleven non-CVs are shown in Figs 6 and 7, and we discuss the likely nature of these systems in Section 5.2. Lastly, an additional 13 published CV candidates were observed by SDSS-V, but their spectra were unusable (Table D1).

5.1 New CVs

Inspection of Fig. 5 shows that amongst the ZTF light curves of the eight new CVs, there is only one outburst (J0635 + 0303) that is very likely a reason why these systems have so far escaped attention.

5.1.1 J0006 + 0121

The spectrum shows strong Hα emission and a steep decrement in the higher lines of the Balmer series. The double-peaked morphology of Hα is evidence of an accretion disc seen at moderately high orbital inclination. The continuum rises towards the blue, which, together with the broad Hγ and Hδ absorption lines, is interpreted as being dominated by the emission of the white dwarf. This assumption is consistent with the location of J0006+0121 within the white dwarf cooling sequence. The fact that the white dwarf is visible, combined with the absence of outbursts in the CRTS and ZTF light curves, indicates a low mass transfer rate. No spectroscopic features of the donor star are detected in the red part of the spectrum and the weak infrared peak in the SED plot is suggestive of a brown dwarf companion. We classify this as a WZ Sge.

A periodogram computed from the radial velocities measured from the eight individual SDSS spectra displays a number of possible periods separated by 1-d aliases. While the SDSS spectroscopy is not sufficient to unambiguously identify the orbital period, the most likely values from THE JOKER periodogram are 1.434(3) h, 1.525(4) h, and 1.628(4) h, where the uncertainties have been determined from sine fits to the data. We were unable to obtain a period from either the CRTS or ZTF data. If either of the two longer periods represent the true orbital period, this system would likely be a 'period bouncer'.

5.1.2 J0624 + 4007

The spectrum exhibits a steep blue continuum and weak, narrow Hα emission line. The higher Balmer lines display narrow absorption profiles (with a hint of an emission core in Hβ). The ZTF light curve shows the system at constant brightness. With $G_{abs} = 7.35$ and $G_{BP} - G_{RP} = 0.39$, this CV is located near the bottom of the area of the HR diagram populated by nova-like variables (see fig. 6 of Inight et al. 2022). Combining all observational evidence suggests that J0624 + 4007 is a novalike. The relatively faint absolute magnitude suggests that it is either a high-inclination system (i.e. nearly edge-on) or, taking into account the absence of eclipses, one with a relatively low mass transfer rate, or both. We were unable to obtain an orbital period from either the radial velocities or the ZTF photometry.

5.1.3 J0633 + 0303

The spectrum shows strong double-peaked Balmer and He I emission lines on a red continuum. However, the flux calibration of this spectrum is problematic (see Section 3.1), as the system is located in the Galactic plane ($b = -2.7°$) with a maximum reddening of $E(B - V) \simeq 1.1$ along this line of sight (Schlafly & Finkbeiner 2011). However, with a distance of $\simeq 242$ pc,

The system is in front of most of the dust (Lallement et al. 2019), and inspecting the SED plot of J0633 + 0303 reveals that it is a blue object. With that knowledge in mind, the spectrum reveals broad depressions, suggesting that the white dwarf dominates the emission, which is consistent with the position near the white dwarf cooling sequence in the *Gaia* HR diagram and is indicative of a low level of accretion. Analysis of the SDSS-V radial velocities indicates a period of approximately 1.4 h. However, the sampling of
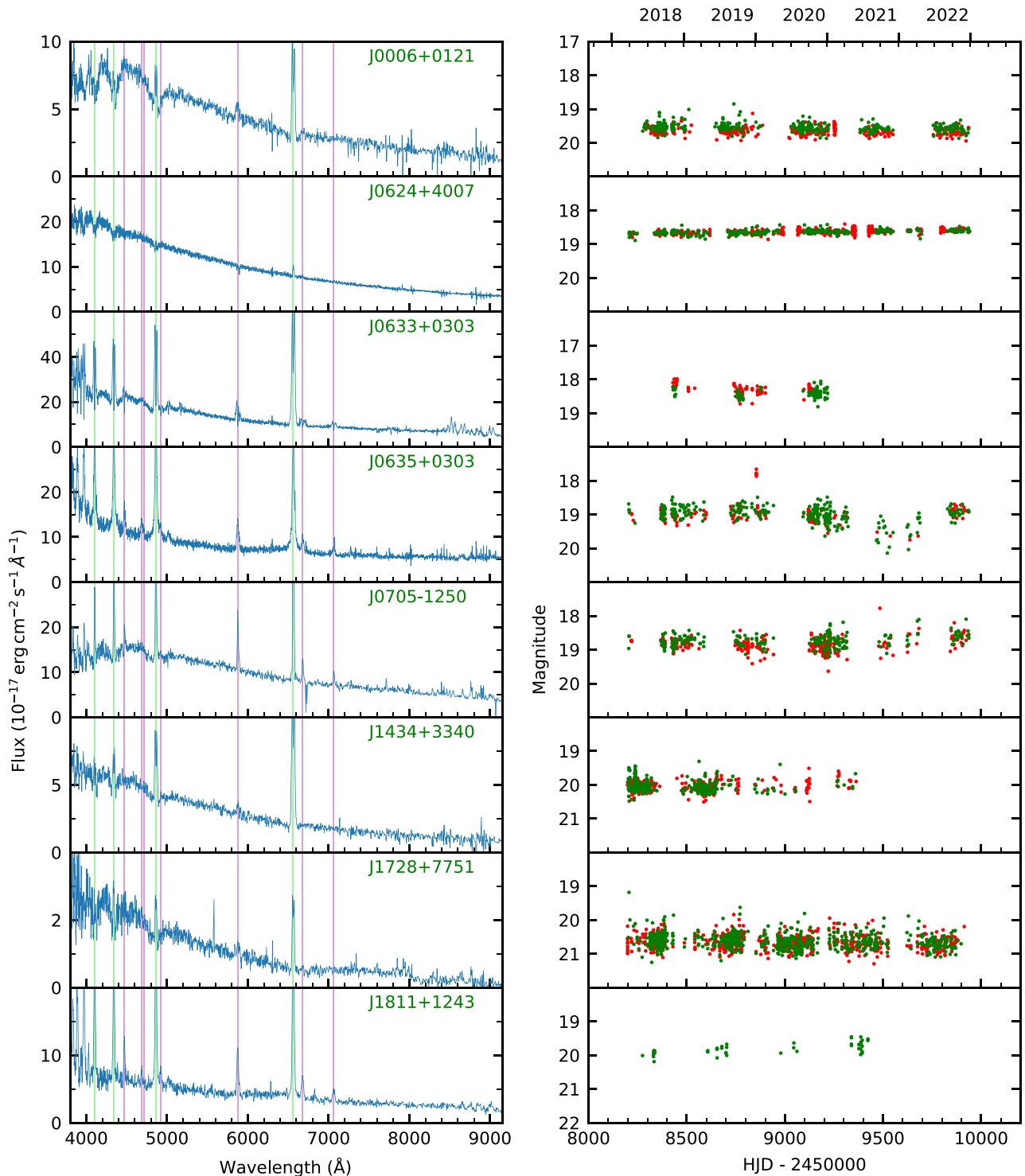
Figure 5. Left-hand panels: Spectra of the eight new CVs discovered by SDSS-V. Right-hand panels: ZTF light curves (*r*- and *g*-band) of the eight new CVs.

the available spectroscopy results in several possible aliases near 1.4 h so that we are unable to unambiguously identify the correct period. The ZTF light curve is relatively sparse and contains no outbursts. The very deep central absorption in the Balmer lines suggests a high inclination, and possibly eclipsing nature of J0633 + 0303. Based on the spectroscopic appearance, period, and absence of outbursts, it is most likely a WZ Sge dwarf nova.

5.1.4 J0635 + 0303

The spectrum shows strong Balmer and He I emission lines. The He II line is very weak. The asymmetric morphology of the emission lines, and their very broad wings suggest that J0635+0303 is a magnetic CV, although the spectrum does not reveal any cyclotron humps. J0635 + 0303 is located in the Galactic plane ($b = -2.2°$) with a maximum reddening of $E(B - V) \simeq 1.5$ resulting in bad
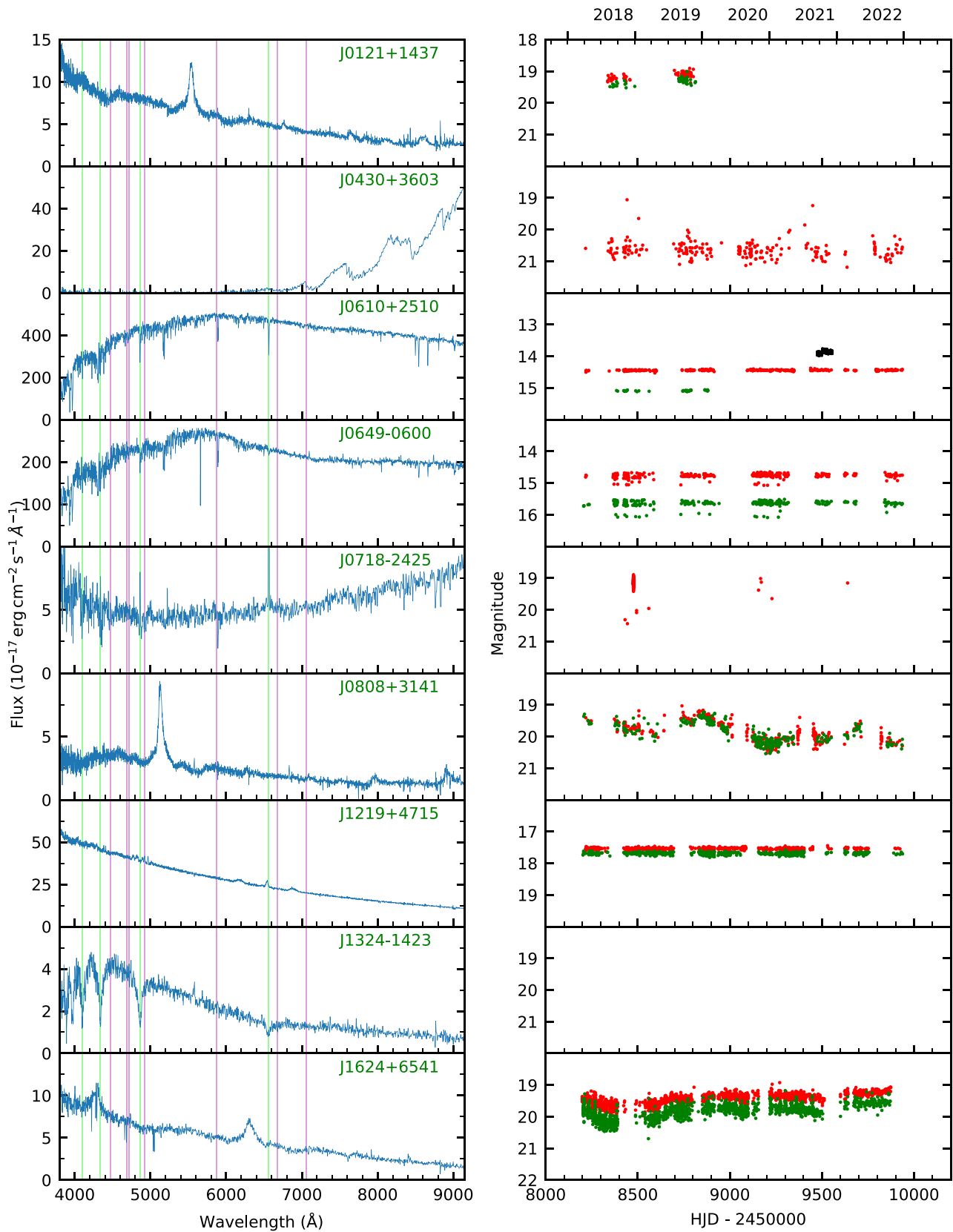
Figure 6. SDSS-V Spectra (left) and (*r*- and *g*-band) ZTF light curves (right) of systems misclassified in the literature as CVs and CV candidates.
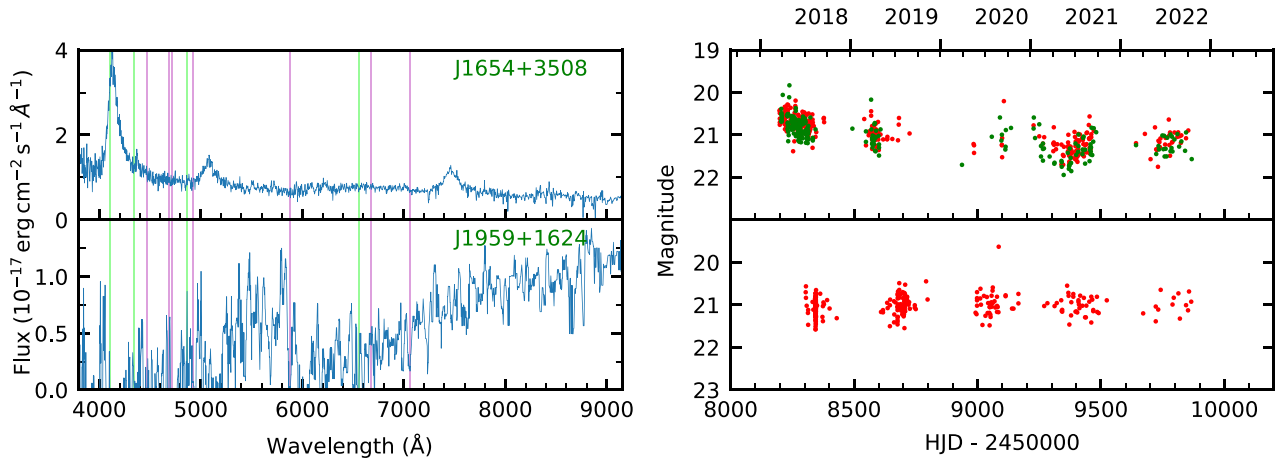
Figure 7. Fig. 6 continued.

flux calibration of the SDSS spectrum. However, with a distance of $\simeq 643$ pc, the CV will only be reddened by $E(B - V) \simeq 0.1$ and, as is evident from the broad-band photometry, it is intrinsically blue. J0635 + 0303 has been detected as an X-ray source in a 1.4 ksec exposure (Evans et al. 2020). The ZTF light curve contains a $\Delta m \simeq 1.3$ outburst at MJD = 58 854, and a dip in its brightness between MJD $\simeq$ 59 200 and 59 800. The ZTF power analysis shows a strong peak at 1.47 h. There are three epochs of good spectroscopic data and using the photometric period as a seed resulted in a period of 1.4717 h. Visual inspection confirms that $P_{orb} = 1.4717(2)$ h is the most likely orbital period. We conclude that J0635 + 0303 is probably a polar.

5.1.5 J0705–1250

The spectrum shows strong Balmer and He I emission lines and broad Balmer absorption lines from the white dwarf, but no sign of the donor. The emission lines are narrow indicating a low inclination. The ZTF light curve does not contain any outbursts. Although there are *Swift* X-ray detections, this system is close (246 pc), and so the detection of X-rays is not necessarily suggestive of it being a magnetic CV. J0705–1250 is located on the white dwarf cooling sequence in the HR diagram. Analysis of the radial velocities measured from five epochs of reasonably good radial velocity data reveals a best-fitting period of 1.4986(1) h. This value is, however, not consistent with ZTF periodograms that reveal potential periods of 2.34 and 2.13 h. Given the somewhat mixed set of characteristics, we classify J0705–1250 as a generic CV, and we encourage follow-up studies of this system to accurately determine the orbital period, and stringently rule out a magnetic nature of the white dwarf.

5.1.6 J1434 + 3340

This object was identified as an optical counterpart to *Chandra* CXOXB J143435.3 + 334048 by Brand et al. (2006) who were searching for active galatic nucleus. It has double peaked Balmer and He I lines but no evidence of He II at 4686 Å. The white dwarf absorption lines are visible, but there is no signature of the donor in either the spectrum or the SED. J1434 + 3340 sits on the white dwarf cooling sequence in the HR diagram. We could not recover any radial velocity variation. There are no outbursts in the CRTS and ZTF light curves, and the photometric data do not reveal any periodicity. We

conclude that this is a WZ Sge and would expect it to have a period close to the period minimum.

5.1.7 J1728 + 7751

The spectrum shows double-peaked Balmer and He I emission lines on top of a blue continuum. The white dwarf absorption lines are visible, but there is no spectroscopic detection of the donor. The ZTF light curve shows a single bright outlier which seems insufficient to qualify as an outburst detection. We could neither recover any radial velocity variations from the SDSS-V spectra, nor could we derive a period from the ZTF data. J1728 + 7751 is located close to the white dwarf cooling sequence in the HR diagram, and it is probably a WZ Sge.

5.1.8 J1811 + 1243

The spectrum shows strong Balmer, He II and He I emission lines, and there is no sign of either the white dwarf or the donor. The absence of a spectroscopic signature of the donor suggests that the system is below the period gap. J1811 + 1243 is closer to the white dwarf cooling sequence than the main sequence in the HR diagram, indicating a relatively low accretion rate. The ZTF light curve contains only 32 observations; there are no CRTS observations. We have seven radial velocity measurements over three epochs of varying SNR but cannot derive a reliable period. We conclude that this is probably a SU UMa.

5.2 Misclassified systems

Analysis of the SDSS-V spectra, ancillary data, and the literature demonstrates that 11 systems (Table 3) were previously misclassified as CVs or CV candidates. Their SDSS-V spectra and ZTF light curves are shown in Figs 6 and 7, and we briefly discuss their most likely nature below.

5.2.1 J0121 + 1437

This system was detected as a transient by CRTS (MLS 160708:012156 + 143737). The spectrum shows a broad emission line typical of a quasar and is likely to be Lyα at $z \simeq 3.5$.

5.2.2 J0430 + 3603

This object was identified as a transient by MASTER (OT J043017.84 + 360326.9, Shurpakov et al. 2014) and subsequently categorized as a U Gem dwarf nova by VSX Watson et al. 2006. The SDSS-V spectrum reveals a very red slope with strong TiO absorption bands, characteristic of an M-dwarf. The available broadband photometry is very red and J0430+3603 is located above the location of single low-mass main-sequence stars in the HR diagram. J0430 + 3603 has a *Spitzer* detection, which was categorized as a young stellar object (YSO) in Broekhoven-Fiene et al. (2014), which appears consistent with its location in the HR diagram. This object was in the footprint of *GALEX* but was not detected in the ultraviolet. We conclude that J0430 + 3603 is a single star, and the transient detected by MASTER was very likely a flare.

5.2.3 J0610 + 2510

This object was first identified as a short period variable (NSV 2853) in 1949, and it is classified in VSX as a U Gem dwarf nova. Haefner, Fiedler & Rau (1996) obtained CCD photometry for 2 h and concluded that it was not a CV. Liu & Hu (2000) also obtained photometry and concluded that it was a late G-type star – which is consistent with its position on the HR diagram. The ZTF and *TESS* light curves do not show outbursts, and we concur with Liu & Hu (2000) that it is not a CV. The reason why it was classified as a variable star in the first place remains unclear.

5.2.4 J0649–0600

This object, BEST-II lra2b_01098, was found to be variable by Kabath et al. (2009), and it is classified in VSX as a δ Cepheid type star or a CV. The SDSS-V spectrum of J0649 − 0600 resembles a G/K-spectral type and does not contain any emission lines. Within the *Gaia* HR diagram, J0649–0600 is located in the sub-giant branch. The ZTF light curve exhibits 0.4 mag peak-to-peak variability, and an AOV analysis of the ZTF data reveals this system to be an eclipsing binary with a period of 9.8 d. We conclude that J0649 − 0600 is not a CV.

5.2.5 J0718–2425

This object was identified as a *Gaia* alert (Gaia18ajg, Hodgkin et al. 2021) and classified as a U Gem type by VSX. The system is relatively red ($G_{BP} - G_{RP} \simeq 2$), is located slightly above the main sequence in the HR diagram, and exhibits a strong infrared excess, and the SDSS spectrum displays very narrow emission lines. All the observational evidence suggests that J0718 − 2425 is not a CV, and that it may be a YSO.

5.2.6 J0808 + 3141

This object was identified as a transient by MASTER (OT J080826.00 + 314125.6, Balanutsa et al. 2015) and subsequently categorized as a CV by VSX. The spectrum shows a broad emission line typical of a quasar and is likely to be Lyα at $z \simeq 3.2$.

5.2.7 J1219 + 4715

This object was classified as a CV candidate based on earlier SDSS spectroscopy (Szkody et al. 2006) because of its weak Hα emission and blue continuum, characteristics of a CV in outburst or a novalike. However, Gänsicke et al. (2020) subsequently classified J1219 + 4715 as a single magnetic white dwarf with Zeeman-split Balmer emission lines, similar to the enigmatic white dwarf GD356 (Greenstein & McCarthy 1985).

5.2.8 J1324–1423

This object was identified by a transient in *Gaia* alerts as Gaia17aoi and has been categorized by VSX as a U Gem. Pala et al. (2020) raised concerns about the astrometry. The spectrum resembles that of a white dwarf, with no emission lines, which is consistent with its position in the HR diagram. The SED shows no evidence of a red component, and we conclude that this is not a CV but a single white dwarf, and that the nature of the transient detected by *Gaia* remains elusive.

5.2.9 J1624 + 6541

Gaia identified this system as a transient, Gaia16aat, which was subsequently classified as a CV by VSX. The spectrum shows a broad emission line typical of a quasar, which is likely to be Lyα at $z \simeq 4.2$.

5.2.10 J1654 + 3508

This was identified as a transient by CRTS (MLS 160613:165449 + 350804); no follow-up studies are reported in the literature. The spectrum shows a broad emission line typical of a quasar, which is likely to be Lyα at $z \simeq 2.4$. We note that this quasar has a large positive parallax, albeit with a large uncertainty.

5.2.11 J1959 + 1624

This object was identified as a *Gaia* alert (Gaia17bqf) and classified as a U Gem dwarf nova by VSX. All other *Gaia* observations were non-detections. It is located near the region of the main-sequence occupied by M0 types in the *Gaia* HR diagram. The SDSS-V spectrum is very noisy and shows no indication of emission lines. The available broad-band photometry is consistent with a single cool stellar object without any ultraviolet excess. We conclude that J1654 + 3508 is not a CV, and that the brightening detected by *Gaia* was most likely due to a stellar flare.

6 DISCUSSION

6.1 Period bouncers

The standard evolutionary model of CVs (see Inight et al. 2023 for a recent summary) predicts that nuclear burning in the donor star stops once mass transfer has eroded its mass to $\simeq 0.06 M_\odot$, at which point the star's structure becomes dominated by electron degeneracy, and it becomes a brown dwarf. As a consequence of the now inverted mass–radius relation, the orbital separations and periods increase as they continue their evolution. CVs that have passed the period minimum are colloquially referred to as 'period bouncers'. QZ Lib is an excellent example of a period bouncer, having an orbital period of 92.7 min, but a very cool ($\lesssim 1700$ K) donor star (Pala et al. 2018). The evolution of CVs near the period minimum has been one of the areas where theory and observations show the largest discrepancies:

(1) The predicted location of the period minimum fell short of the observed value by about 10 per cent (Kolb & Baraffe 1999). Assuming some amount of angular momentum loss in addition to

Table 3. Previously known CVs and CV candidates that have been misclassified in the literature.

SDSS name	Alternative name	New category
SDSS J012156.25 + 143737.2	MLS160708:012156 + 143737	Extra galactic
SDSS J043017.85 + 360326.6	MASTER OT J043017.84 + 360326.9	YSO
SDSS J061043.98 + 251031.0	NSV 2853	Star
SDSS J064939.16 − 060005.0	BEST-II lra2b_01098	Detached binary
SDSS J071844.74 − 242546.3	Gaia18ajg	YSO:
SDSS J080826.00 + 314125.3	MASTER OT J080826.00 + 314125.6	Extra galactic
SDSS J121929.32 + 471522.9	SDSS J121929.46 + 471522.8	White dwarf
SDSS J132444.33 − 142335.7	Gaia17aoi	White dwarf
SDSS J162450.04 + 654101.1	Gaia16aat	Quasar
SDSS J165449.45 + 350803.7	MLS160613:165449 + 350804	Extra galactic
SDSS J195919.93 + 162440.3	Gaia17bqf	Star

gravitational wave radiation removes that discrepancy (Patterson 1998; Knigge, Baraffe & Patterson 2011), and this is the currently favoured solution.

(2) As the evolution of CVs not only slows down towards the period minimum but also subsequently reverses towards longer periods, an accumulation of systems near the period minimum, the so-called 'period minimum spike' has been a firm prediction of all CV population models. Yet observed CV samples consistently fail to exhibit this feature (e.g. King, Schenker & Hameury 2002), and it was only the SDSS CV sample that confirmed the existence of the period minimum spike (Gänsicke et al. 2009). The key conclusion was that the earlier CV samples were too shallow to capture a sufficiently large number of the faint population of period-minimum CVs.

(3) Evolutionary models predict that a large proportion of CVs are period bouncers: Kolb (1993) suggested that 70 per cent of all CVs are period bouncers, whilst Goliasch & Nelson (2015) predicted 38–60 per cent and table 1 of Belloni et al. (2018) suggests 75 per cent. Despite much observational effort, the roster of known period bouncers remains small: Patterson (2011) discussed 22 candidates among the known CVs; Pala et al. (2020) estimated a period bouncer fraction of 7–14 per cent within the 150 pc CV sample; and Inight et al. (2023) concluded that only 0.7 per cent of all the CVs observed by SDSS I to IV were period bouncers. Hernández Santisteban et al. (2018) used the SDSS Stripe 82 and Palomar Transient Factory photometry for an unbiased search of eclipsing period bouncers and derived an upper limit on their space density of $\lesssim 2 \times 10^{-5}$ pc^{-3}.

The dedicated spectroscopic follow-up of CV candidates carried out by SDSS-V obtained nearly complete spectroscopy of period-bounce candidate systems, which we use below to derive a more stringent estimate of the space density of period bouncers.

We collected a sample of confirmed and high-confidence period bouncers (Table 4) that have SDSS spectroscopy, either obtained as part of SDSS I to IV (Inight et al. 2023) or SDSS-V (this paper), and used their *Gaia* astrometry and photometry to identify their location within the HR diagram. We found that period bouncers are closely clustered near the cooling sequence of single white dwarfs (Fig. 8), which is unsurprising as their optical spectra are dominated by the flux from the white dwarf, with only small contributions from the accretion discs and negligible amounts of light from the brown dwarf donors. A number of the systems in Table 4 stood out as outliers from this clustering. Upon closer inspection, we found that these outliers have poor *Gaia* astrometry, and consequently, we removed all systems with $\Delta\varpi/\varpi \geq 0.2$ from the definition of the location of period bouncers in the HR diagram. We then

computed the minimal enclosing ellipse (Welzl 1991) that contains the known period bouncers, where we accounted for the observed uncertainties by displacing each system within its 1σ errors. We then assume that hitherto undiscovered period bouncers have similar absolute magnitudes and colours to the ones that are known already. We believe that this is a reasonable assumption as the white dwarf temperature is set by the accretion rate (Townsley & Gänsicke 2009), and there is so far no known CV with a quiescent white dwarf temperature $\lesssim 9500$ K (Sion & Godon 2015). Theoretical models predict that the accretion rate should rapidly decrease as systems evolve back from the period minimum, and hence longer period period bouncers should have significantly cooler white dwarfs. However, no such system is known, which means that, if they exist, they are undetectable by photometric variability (including outbursts or eclipses), X-ray emission, or emission lines, as plenty of data are available to find at least a handful of these hypothetical systems.

Next, we analysed the number of targets within the mwm_wd carton that fall within this ellipse, and the number of spectroscopic observations of these targets carried out by SDSS-V. We made use of only the mwm_wd carton as it provides good coverage of the HR diagram location occupied by period bouncers, has the cleanest selection rules, homogeneously covers the entire SDSS-V footprint, and has a well-defined ($G \leq 20$ mag) magnitude limit. We found 1376 mwm_wd targets within the ellipse defined by the known period bouncers, of which 1132 were observed during the SDSS-V plate program, i.e. the correction factor to account for the incompleteness of the spectroscopic observations is $C_{\mathrm{orr}} = 1.22$. Amongst these 1132 observed targets, eight displayed emission lines, and these were classified using the methodology described in Section 4.1.1. From these eight, we identified only one candidate period bouncer (based on the combination of the signature of the white dwarf being visible in the spectrum, the donor not being visible in the spectrum, the SED being consistent with a brown dwarf donor and the orbital period significantly greater than the period minimum): J0006 + 0121 with a period of 91 min ($N_{\mathrm{obs}} = 1$).[2]

We estimated the space density of period bouncers using the technique described in section 6.4 of Inight et al. (2023). We first concluded from inspection of Fig. 8 that all period bouncers would have an absolute magnitude $G_{\mathrm{abs}} \leq 12.25$, yielding a limiting distance of $R_{\mathrm{lim}} = 355$ pc. Following Inight et al. (2023), we assumed a scale

---

[2]The plate program obtained spectroscopy of three additional candidate period bouncers, J0233+0050 ($P_{\mathrm{orb}} = 96$ min), J0845+0339 with a period of 87 min, and J1434+3340 (no P_{orb}), which are, however, all too faint to be included in the mwm_wd carton.

Table 4. Period bouncers (with candidates shown in italics) from SDSS I to IV and SDSS-V. This sample was used (excluding those with bad astrometry) to characterize the location of period bouncers in the HR diagram (Fig. 8). Where the donor mass is not known, the ratio of donor mass to white dwarf mass (q) is provided – reasonable values for the white dwarf mass imply donor masses consistent with being a period bouncer.

| SDSS name	Other name	*Gaia* G	Distance (pc)	Bad astrometry	P_{orb} (h)	Donor mass ($M_\odot$)	Reference
J0006 + 0121		19.64	352		1.52		This work
J0233 + 0050	HP Cet	20.16	683	*	1.6		This work
J0845 + 0339	V498 Hya	20.83	1635	*	1.45		This work
J1434 + 3340		20.14	363				This work
J0058-0107	ASASSN-16iw			*	1.56	$q = 0.079$	Kato et al. (2017)
J0804 + 5103	EZ Lyn	17.79	143		1.43	0.042	Amantayeva et al. (2021)
J0843 + 2751	EG Cnc	18.77	187		1.44	0.02	Patterson et al. (1998)
J0904 + 4402	FV Lyn	19.42	335		1.67		Inight et al. (2023)
J1035 + 0551		18.78	196		1.37	0.06	Littlefair et al. (2006a)
J1057 + 2759		19.54	355		1.51	0.044	McAllister et al. (2017)
J1212 + 0136	V379 Vir	17.98	152		1.47		Farihi, Burleigh & Hoard (2008)
J1216 + 0520		20.11	377		1.65	<0.04	Southworth et al. (2006)
J1255 + 2642	MT Com	19.21	347		1.99	<0.05	Patterson, Thorstensen & Kemp (2005)
J1433 + 1011		18.55	232		1.3	0.0571	Savoury et al. (2011)
J1435 + 2336		18.62	209		1.3		Pala et al. (2022)
J1507 + 5230	OV Boo	18.15	212		1.11	0.056	Littlefair et al. (2007)
J2131 − 0039	QZ Aqr			*	1.67		Inight et al. (2023)
J2304 + 0625	KX Psc	20.91		*	1.62	$q = 0.053$	Nakata et al. (2014)
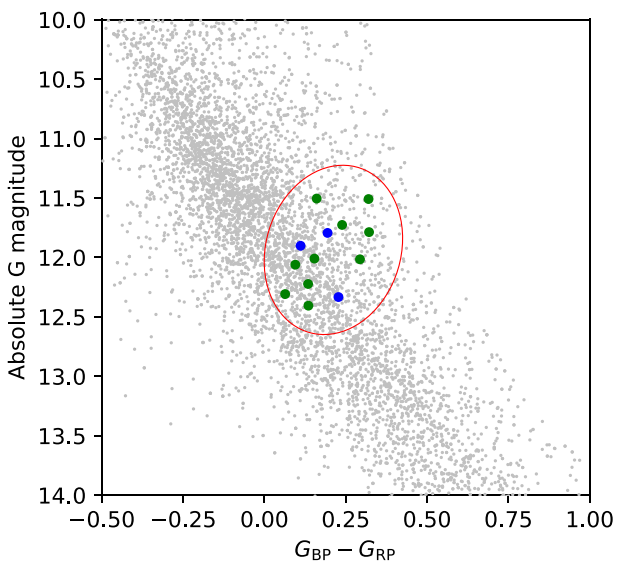
Figure 8. HR diagram of period bouncers (green dots) and candidates (blue dots) with reliable parallaxes ($\Delta\varpi < 0.2 \times \varpi$) taken from Inight et al. (2023) and this paper (see Table 4). The red contour shows the minimal enclosing ellipse (centred on $G_{BP} - G_{RP} = 0.193$, $G_{abs} = 11.921$ with semimajor and minor axes of 0.574 and 0.1159 and rotated by 96.70°) containing the known period bouncers, allowing for 1σ uncertainties in their *Gaia* parameters. The grey dots are the targets of the mwm_wd carton within the footprint of the 236 SDSS-V plates analysed here.

height of 450 pc as period bouncers are an old population. Next, we determined the SDSS-V sky coverage from the 236 plates on which the 1132 mwm_wd targets were observed. HEALpixs were then used to find the sky coverage of these 236 plates by accounting for overlaps and hence the effective volume of the magnitude limited mwm_wd sample contained within the ellipse defined by the known period bouncers.

Taken together, these assumptions yielded a space density $\rho_0 \simeq 0.2 \times 10^{-6}$ pc^{-3} for period bouncers. Estimates for the composite space density of all sub-types of CVs range from $\rho_0 = 4.8 \times 10^{-6}$ pc^{-3} (Pala et al. 2020) to $\rho_0 = 7.8 \times 10^{-6}$ pc^{-3} (Inight et al. 2023) implying that accreting period bouncers only account for about 3 per cent of CVs.

From the above analysis, we can only conclude that the large number of period bouncer predicted by CV models either do not exist, or that the majority of them look so distinctly different from the small sample of known period bouncers that they escape spectroscopic (our analysis) and photometric (Hernández Santisteban et al. 2018) detections. Our conclusions echo those of Patterson (1998), *'It is probably necessary to have some means of destroying CVs before they reach the predicted very high space densities'*. Possible scenarios to 'destroy' CVs include either a merger, maybe as a result of a final classical nova eruption (e.g. via consequential angular momentum loss, Nelemans et al. 2016; Schreiber, Zorotovic & Wijnen 2016), or the secondary contracting within its Roche lobe, thereby terminating mass transfer. The latter option was suggested by Patterson (1998), arguing that the final state of CVs may be white dwarfs with detached, planet-like companions – and the ultimate test of that hypothesis would be a more sensitive survey for apparently single white dwarfs eclipsed by their (at optical wavelengths) invisible ultra-low-mass companions.

6.2 Orbital period distribution

We have obtained periods for 72 of the 118 CVs in the SDSS-V plate survey. The main reasons why the remaining systems have no period measurements are due to either a low inclination (which will reduce the amplitude of any orbital modulation), faintness (i.e. low signal-to-noise ratio of the time-series photometry or spectroscopy), or sparse sampling of the available time-series data. With the possible exception of low $\dot{M}$ short-period CVs (which do not have much orbital modulation from the hot spot and are inherently fainter), these factors are not likely to correlate with the period.

The orbital period distribution of the SDSS-V CVs is shown in Fig. 9, where it is compared to that of the Ritter & Kolb (2003) sample, which is a very heterogeneous collection of CVs, and the
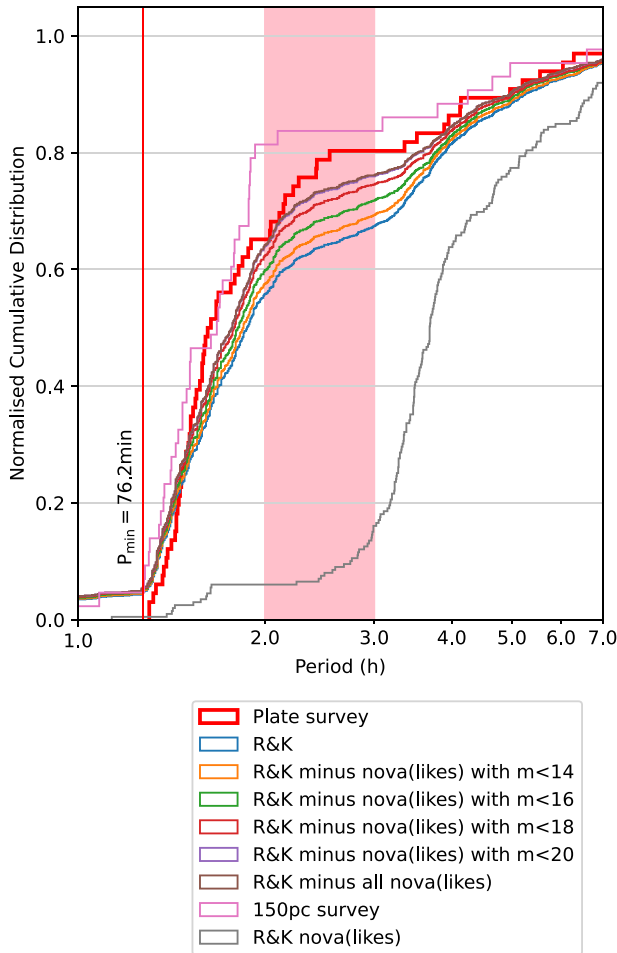
Figure 9. Cumulative distribution of the orbital periods of the CVs observed by SDSS-V, compared to those of the Ritter & Kolb (2003) catalogue of CVs and of the 150 pc volume-limited survey (Pala et al. 2020). The period minimum (red line) and 'period gap' (pink rectangle) are indicated (see text for details). We also include the period distribution of Ritter & Kolb (2003) with classical novae and novalikes removed, for a range of limiting magnitudes, as well as the period distribution of classical novae and novalikes alone, demonstrating the selection effect of these intrinsically bright objects.

150 pc volume-limited sample of Pala et al. (2020). The period gap, which has been a defining feature of the observed period distribution of CVs and motivated the widely accepted idea of 'disrupted magnetic braking' (Rappaport, Verbunt & Joss 1983; Howell, Nelson & Rappaport 2001; Schreiber et al. 2010), is at best marginally detected in the SDSS-V sample, which is in clear contrast with the period distribution of the CVs from the Ritter and Kolb (R&K) catalogue. Classical novae (post-eruption) and nova-like variables are inherently bright (fig. 15 of Inight et al. 2023) and are overrepresented in Ritter & Kolb (2003). They also typically have orbital periods above $\simeq 3$ h. We therefore removed classical novae and novalikes from Ritter & Kolb (2003), and the resulting period distribution (see Fig. 9) is then closely aligned with that of the SDSS-V sample. To illustrate the effect of different limiting magnitudes, we also include period distributions of the R&K sample cut at $m < 14, 16, 18,$ and 20, which clearly shows that different limiting magnitudes have the largest effect in the $\simeq 3$–4 h orbital period range.

In order to assess the statistical significance of the period distributions of different observed CV populations, we carried out the two-sample Kolmogorov–Smirnov (KS) test (Hodges 1958) pairwise between two volume-limited samples, the 150 pc sample of Pala et al. (2020), the 300 pc 'Gold' sample of (Inight et al. 2021), two magnitude-limited samples, the SDSS-V CVs analysed in this paper, and those in the Ritter & Kolb (2003) catalogue (R&K). We truncated the period distributions for $P_{orb} < 75$ min to remove the AM CVn systems, as we are interested in comparing the properties of 'normal' CVs with hydrogen-rich donor stars. The KS test evaluates the likelihood of the samples being compared sharing the same underlying orbital period distribution. The KS statistic measures the maximum difference in the cumulative probability distributions, and we used the SCIPY.STATS.KS_2SAMP function to calculate a p-value. For instance, a p-value of less than 0.05 implies that the surveys are drawn from different distributions with 95 per cent confidence.

The main difference between the 150 and 300 pc samples is that the former has a substantially higher completeness (77 ± 10 per cent) than the latter ($\simeq 50$ per cent). However, the 150 pc sample is much smaller (42 systems) than the 300 pc sample (151 systems). The cumulative distributions of the two samples are visually very similar (right-most panel in Fig. 10), and the KS indicates a very low probability of the two being drawn from different underlying populations. We hence conclude that despite the lower completeness, the 300 pc sample is representative of the intrinsic CV population.

Comparing the period distribution of the SDSS-V CVs to those of the 150 and 300 pc samples (third and second panels from the right in Fig. 10, respectively) reveals a shortfall of systems around $P \simeq 2$ h; however, the p-values determined from the KS tests are sufficiently large that there is no statistical evidence that the period distribution of the SDSS-V CV sample differs from those of the volume-complete ones.

However, the 300 pc CVs and the R&K sample (second panel from the left in Fig. 10) have very clearly distinct period distributions: the R&K sample shows distinct changes in the slope at $\simeq 2$ h and $\simeq 3$ h, which Knigge (2006) interpreted as clear signatures of the lower and upper edge of the period gap, respectively. In contrast to this, the 300 pc CV sample shows a steep break in the slope of the cumulative distribution at $\simeq 2$ h, but much less-pronounced structure at longer orbital periods – there is a small hint of a break in the slope at $\simeq 4$ h. Based on the KS test, the two samples have intrinsically different period distributions at a very high significance (> 99.9 per cent).

Similarly, the SDSS-V CVs and the R&K sample (left-most panel in Fig. 10) differ distinctively, with the number of short-period SDSS-V CVs increasing well beyond the canonical $\simeq 2$ h lower edge of the period gap, and not exhibiting a strong break at $\simeq 3$ h. Based on the KS test, the two samples have intrinsically different period distributions at a very high significance ($\simeq 98$ per cent). Whereas we stress that the SDSS-V sample is neither complete nor subject to a homogeneous selection of the CV candidates that were targeted for spectroscopy, it approximates the inherent period distribution revealed by the volume-limited samples better than the R&K sample – most likely because of the large limiting magnitude of SDSS.

We conclude that the observational evidence for the period gap is primarily based on the very heterogeneous R&K sample and is linked to the large fraction of classical novae and nova-like variables within that sample. If the period gap is indeed an intrinsic feature of the CV population and a signature of disrupted magnetic braking, its early identification (Whyte & Eggleton 1980) would be based on a 'lucky' selection effect among the earliest CV discoveries.

We note in passing that the SDSS-V period distribution, as well as those of the 300 pc sample, show a slight flattening between
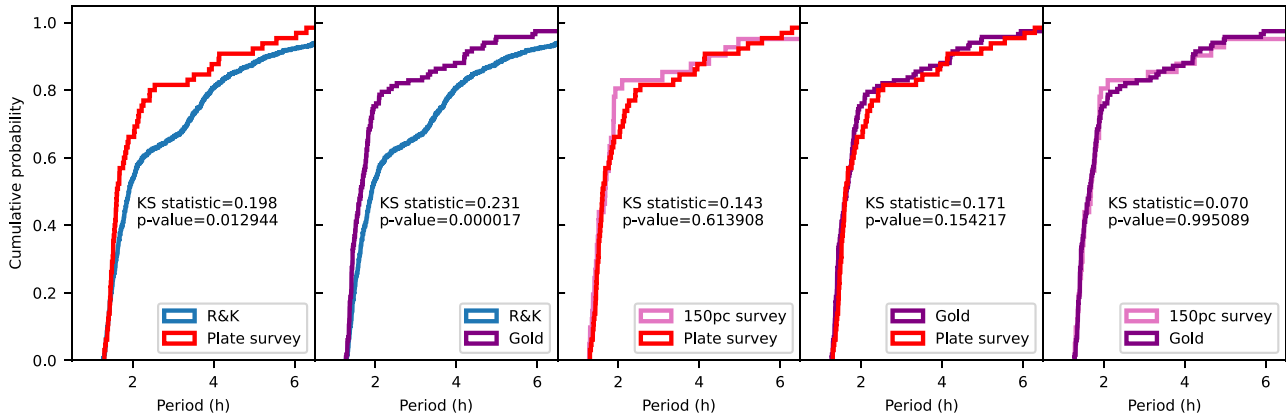
Figure 10. We used the two-sample KS test (Hodges 1958) to compare pair-wise the cumulative orbital period distributions of the CVs observed by SDSS-V (Plate survey), the CVs in the Ritter & Kolb (2003) catalogue (R&K), the CVs in the volume-limited 150 pc sample of Pala et al. 2020 (150 pc), and the CVs in the volume-limited 300 pc 'Gold' sample from Inight et al. 2021 (Gold). The KS tests demonstrate that the underlying period distributions of both the Gold sample and the SDSS-V CVs differ from that of R&K at a highly significant level. In contrast, there is no evidence that the period distributions underlying the SDSS-V, 150 and 300 pc samples differ.

Table 5. The CV sub-types of the new and previously known systems.

CV type	Previously known	New	Total
U Gem	26	0	26
ER UMa	3	0	3
SU UMa	36	1	37
WZ Sge	9	4	13
Z Cam	1	0	1
AM CVn	3	0	3
Classical nova	5	0	5
Novalike	1	1	2
Polar – AM Her	14	1	15
Intermediate polar – DQ Her	2	0	2
Magnetic CV	1	0	1
Dwarf nova	7	0	7
Unclassified	2	1	3
Total	**110**	**8**	**118**

$\simeq 3$ h and $\simeq 5$ h, which is consistent with the predictions of Schreiber et al. (2021) for CVs where the formation of magnetic white dwarfs undergoes a detached phase within that period range, resulting in a decrease in the number of accreting CVs. However, we stress that a larger volume-limited CV sample is required before this feature would be sufficiently secure to provide robust support to the model of Schreiber et al. (2021).

Finally, it is worth noting that the orbital periods of the new CVs found by SDSS-V, where we were able to obtain unambiguous measurements, are all below 94 min, which is typical of old, low accretion rate systems. This reinforces the findings of Gänsicke et al. (2009) and suggests that SDSS-V will continue to increase the proportion of short-period CVs among the known CV population.

6.3 CV sub-types

The distribution of the new and previously known CVs is given in Table 5. Taken in conjunction with their distribution in the HR diagram (Fig. 11), we notice that the new discoveries include a nova-like variable in the expected area (see fig. 8 of Inight et al. 2021). All of the other new discoveries are close to the white dwarf cooling sequence, i.e. the area associated with short-period
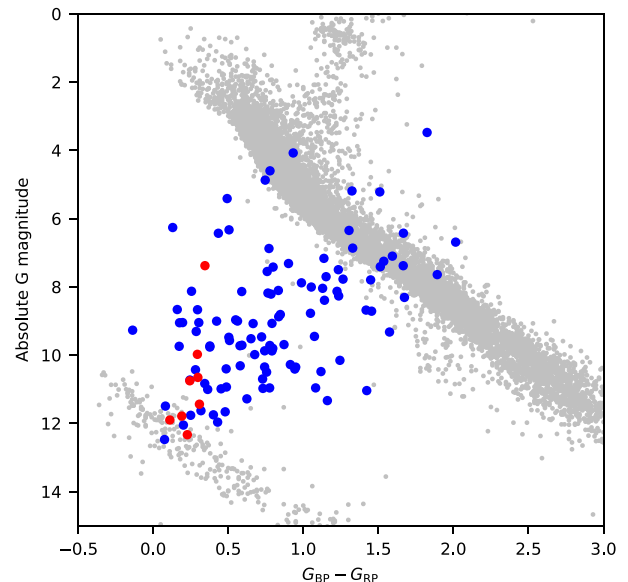

Figure 11. HR diagram showing the 110 previously known CVs in blue and the eight new discoveries in red. The grey dots are an astrometrically clean sample of *Gaia* objects chosen to outline the main sequence and the white dwarf cooling sequence.

CVs with low accretion rates, experiencing infrequent outbursts. This demonstrates the importance of a spectroscopic survey that compensates for the traditional bias of CV searches based on large-amplitude photometric variability. In passing, we note that there are 17 magnetic CVs (14 per cent of the total) in the SDSS-V CV sample, which is similar to the fraction found in the SDSS I to IV sample (Inight et al. 2023), but lower than in the volume-limited 150 pc sample, probably due to the, on average, lower accretion rates in polars when compared to non-magnetic CVs (Webbink & Wickramasinghe 2002; Araujo-Betancor et al. 2005).

7 SUMMARY

SDSS-V is, for the first time, carrying out a dedicated survey of white dwarfs, both single and in binaries. We have analysed the SDSS-V spectra of CVs and CV candidates observed as part of the final plug-plate operations of SDSS, and we discovered eight new CVs. None of the new CVs displays noticeable changes in brightness in their ZTF light curves, underlining the selection effects in existing CV samples that are largely based on photometric variability, and hence the importance of unbiased spectroscopic surveys. We did not discover any new CVs within 150 pc, which is consistent with the relatively high completeness of this volume-limited sample (Pala et al. 2020).

SDSS-V also observed 110 previously known CVs and CV candidates. For 53 of these, the SDSS data represent the first spectroscopic confirmation of their CV nature. Vice versa, the SDSS-V spectroscopy disproves the CV nature of 11 systems that were previously classified as CVs or CV candidates.

We measured 21 new orbital periods from the analysis of radial velocities and time-series photometry. The period distribution of the SDSS-V CV sample does not provide strong evidence for a period gap, which contrasts strongly with the orbital period distribution of the large, but very heterogeneous (Ritter & Kolb 2003) sample. We suggest that future modelling of the CV population should aim to reproduce the period distribution of well-defined samples.

Lastly, but most importantly, we demonstrate that it is unlikely that there is a large population of period bounce CVs awaiting discovery, which represents a major challenge to CV evolution theory. Whilst we cannot totally rule out the possibility of hypothetical period bouncers with a radically different appearance from the handful of known systems, we consider this scenario improbable. The implications are, most likely, that CVs that evolve past the period minimum either get destroyed (e.g. by a merger) or become detached and therefore very difficult to detect. The Legacy Survey of Space and Time survey will provide an opportunity to search for a population of cool white dwarfs that are eclipsed by planet-mass and size objects with periods of $\sim$80–120 min.

SDSS-V will continue to survey both the northern and southern hemisphere for single and binary white dwarfs, and the growing sky coverage will provide increasingly stronger constraints on the intrinsic properties of the Galactic CV population.

DATA AVAILABILITY

SDSS-V data will be publicly available at the end of the proprietary period. The reduced LT light curves presented here will be shared upon reasonable request to the corresponding author. The other data

used in this article are available from the sources referenced in the text.

REFERENCES

Almeida A. et al., 2023, ApJS, 267, 44

Amantayeva A., Zharikov S., Page K. L., Pavlenko E., Sosnovskij A., Khokhlov S., Ibraimov M., 2021, ApJ, 918, 58

Anderson S. F. et al., 2005, AJ, 130, 2230

Antipin S. V., Kroll P., 2003, Inf. Bull. Var. Stars, 5461, 1

Araujo-Betancor S., Gänsicke B. T., Long K. S., Beuermann K., de Martino D., Sion E. M., Szkody P., 2005, ApJ, 622, 589

Arjyotha S., Aungwerojwit A., Gänsicke B. T., Marsh T., Rodríguez-Gil P. R., 2009, in Murphy S. J., Bessell M. S., eds, ASP Conf. Ser. Vol. 404, The Eighth Pacific Rim Conference on Stellar Astrophysics: A Tribute to Kam-Ching Leung. Astron. Soc. Pac., San Francisco, p. 272

Aviles A. et al., 2010, ApJ, 711, 389

Bailer-Jones C. A. L., Rybizki J., Fouesneau M., Mantelet G., Andrae R., 2018, AJ, 156, 58

Bailer-Jones C. A. L., Rybizki J., Fouesneau M., Demleitner M., Andrae R., 2021, AJ, 161, 147

Balanutsa P. et al., 2013, Astron. Telegram, 5676, 1

Balanutsa P. et al., 2015, Astron. Telegram, 8426, 1

Bellm E. C. et al., 2019, PASP, 131, 018002

Belloni D., Schreiber M. R., 2023, preprint (arXiv:2303.08997)

Belloni D., Schreiber M. R., Zorotovic M., Iłkiewicz K., Hurley J. R., Giersz M., Lagos F., 2018, MNRAS, 478, 5626

Bertin E., Arnouts S., 1996, A&AS, 117, 393

Blanton M. R., Lin H., Lupton R. H., Maley F. M., Young N., Zehavi I., Loveday J., 2003, AJ, 125, 2276

Boyd D., Denisenko D., Koff R., Miller I., Staels B., 2011, J. Br. Astron. Assoc., 121, 233

Brand K. et al., 2006, ApJ, 641, 140

Breedt E., Gänsicke B. T., Girven J., Drake A. J., Copperwheat C. M., Parsons S. G., Marsh T. R., 2012, MNRAS, 423, 1437

Breedt E. et al., 2014, MNRAS, 443, 3174

Broekhoven-Fiene H. et al., 2014, ApJ, 786, 37

Bruch A., 1989, A&AS, 78, 145

Bruch A., Schimpke T., 1992, A&AS, 93, 419

Bruch A., Fischer F. J., Wilmsen U., 1987, A&AS, 70, 481

Campbell R. D., Shafter A. W., 1995, ApJ, 440, 336

Carbon D. F., Henze C., Nelson B. C., 2017, ApJS, 228, 19

Carter P. J. et al., 2013, MNRAS, 429, 2143

Carter P. J. et al., 2014, MNRAS, 439, 2848

Chen X., Wang S., Deng L., de Grijs R., Yang M., Tian H., 2020, ApJS, 249, 18

Coppejans D. L., Körding E. G., Knigge C., Pretorius M. L., Woudt P. A., Groot P. J., Van Eck C. L., Drake A. J., 2016, MNRAS, 456, 4441

Cordoni J. P., Gleizes F., Jasniewicz G., 1977, A&A, 55, 307

Cropper M., 1990, Space Sci. Rev., 54, 195

Dawson K. S. et al., 2013, AJ, 145, 10

Deeming T. J., 1975, Ap&SS, 36, 137

Delgado A., Harrison D., Hodgkin S., Leeuwen M. V., Rixon G., Yoldas A., 2017a, Transient Name Serv. Discovery Rep., 2017-547, 1

Delgado A., Harrison D., Hodgkin S., Leeuwen M. V., Rixon G., Yoldas A., 2017b, Transient Name Serv. Discovery Rep., 2017-925, 1

Delgado A., Harrison D., Hodgkin S., Leeuwen M. V., Rixon G., Yoldas A., 2017c, Transient Name Serv. Discovery Rep., 2017-933, 1

Delgado A., Harrison D., Hodgkin S., Leeuwen M. V., Rixon G., Yoldas A., 2018a, Transient Name Serv. Discovery Rep., 2018-1819, 1

Delgado A., Harrison D., Hodgkin S., Leeuwen M. V., Rixon G., Yoldas A., 2018b, Transient Name Serv. Discovery Rep., 2018-423, 1

Delgado A., Harrison D., Hodgkin S., Leeuwen M. V., Rixon G., Yoldas A., 2019, Transient Name Serv. Discovery Rep., 2019-241, 1

Denisenko D. V., Martinelli F., 2016, preprint (arXiv:1609.08511)

Denisenko D. V., Sokolovsky K. V., 2011, Astron. Lett., 37, 91

Denisenko D. et al., 2012, Astron. Telegram, 4441, 1

Denisenko D. et al., 2014, Astron. Telegram, 6049, 1

Djorgovski S. G. et al., 2011, preprint (arXiv:1102.5004)

Drake A. J. et al., 2009a, ApJ, 696, 870

Drake A. J. et al., 2009b, Astron. Telegram, 2086, 1

Drake A. J. et al., 2014, MNRAS, 441, 1186

Evans P. A. et al., 2020, ApJS, 247, 54

Farihi J., Burleigh M. R., Hoard D. W., 2008, ApJ, 674, 421

Ferrario L., Wickramasinghe D., Bailey J., Buckley D., 1995, MNRAS, 273, 17

Ferrario L., de Martino D., Gänsicke B. T., 2015, Space Sci. Rev., 191, 111

Fremling C., Blagorodnova N., Kupfer T., Neill J. D., Walters R., Cannella C. B., Kulkarni S. R., 2018, Astron. Telegram, 11512, 1

Gaia Collaboration, 2018, A&A, 616, A1

Gänsicke B. T., 2005, in Hameury J. M., Lasota J. P., eds, ASP Conf. Ser. Vol. 330, The Astrophysics of Cataclysmic Variables and Related Objects. Astron. Soc. Pac., San Francisco, p. 3

Gänsicke B. T. et al., 2006, MNRAS, 365, 969

Gänsicke B. T. et al., 2009, MNRAS, 397, 2170

Gänsicke B. T., Rodríguez-Gil P., Gentile Fusillo N. P., Inight K., Schreiber M. R., Pala A. F., Tremblay P.-E., 2020, MNRAS, 499, 2564

Garnavich P., Deal S., 2013, Astron. Telegram, 5178, 1

Gehrels N. et al., 2004, ApJ, 611, 1005

Geier S., Østensen R. H., Nemeth P., Gentile Fusillo N. P., Gänsicke B. T., Telting J. H., Green E. M., Schaffenroth J., 2017, A&A, 600, A50

Gentile Fusillo N. P., Gänsicke B. T., Greiss S., 2015, MNRAS, 448, 2260

Gentile Fusillo N. P. et al., 2019, MNRAS, 482, 4570

Gezari S. et al., 2013, ApJ, 766, 60

Goliasch J., Nelson L., 2015, ApJ, 809, 80

Greenstein J. L., McCarthy J. K., 1985, ApJ, 289, 732

Haefner R., Fiedler A., Rau S., 1996, Inf. Bull. Variable Stars, 4366, 1

Halpern J. P., Thorstensen J. R., 2015, AJ, 150, 170

Hameury J. M., 2020, Adv. Space Res., 66, 1004

Heinze A. N. et al., 2018, AJ, 156, 241

Hernández Santisteban J. V., Knigge C., Pretorius M. L., Sullivan M., Warner B., 2018, MNRAS, 473, 3241

Hodges J. L., 1958, Arkiv for Matematik, 3, 469

Hodgkin S. T. et al., 2020, Transient Name Serv. Discovery Rep., 2020-768, 1

Hodgkin S. T. et al., 2021, A&A, 652, A76

Hoffmeister C., 1966, Astron. Nachr., 289, 1

Homer L. et al., 2005, ApJ, 620, 929

Hou W., Luo A. l., Li Y.-B., Qin L., 2020, AJ, 159, 43

Howell S. B., Nelson L. A., Rappaport S., 2001, ApJ, 550, 897

Inight K., Gänsicke B. T., Breedt E., Marsh T. R., Pala A. F., Raddi R., 2021, MNRAS, 504, 2420

Inight K. et al., 2022, MNRAS, 510, 3605

Inight K. et al., 2023, MNRAS, 524, 4867

Jablonski F. J., Cieslinski D., 1992, A&A, 259, 198

Jayasinghe T. et al., 2018, MNRAS, 477, 3145

Kabath P. et al., 2009, A&A, 506, 569

Kato T. et al., 2009, PASJ, 61, S395

Kato T. et al., 2010, PASJ, 62, 1525

Kato T. et al., 2012, PASJ, 64, 21

Kato T., Nogami D., Baba H., Masuda S., Matsumoto K., Kunjaya C., 2013, preprint (arXiv:1301.3202)

Kato T. et al., 2014a, PASJ, 66, 30

Kato T. et al., 2014b, PASJ, 66, 90

Kato T. et al., 2015, PASJ, 67, 105

Kato T. et al., 2016, PASJ, 68, 65

Kato T. et al., 2017, PASJ, 69, 75

Kepler S. O. et al., 2019, MNRAS, 486, 2169

Kepler S. O., Koester D., Pelisoli I., Romero A. D., Ourique G., 2021, MNRAS, 507, 4646

King A. R., Schenker K., Hameury J. M., 2002, MNRAS, 335, 513

Knigge C., 2006, MNRAS, 373, 484

Knigge C., Baraffe I., Patterson J., 2011, ApJS, 194, 28

Kolb U., 1993, A&A, 271, 149

Kolb U., Baraffe I., 1999, MNRAS, 309, 1034

Kollmeier J. A. et al., 2017, preprint (arXiv:1711.03234)

Kraus A. L., Craine E. R., Giampapa M. S., Scharlach W. W. G., Tucker R. A., 2007, AJ, 134, 1488

Kupfer T. et al., 2018, MNRAS, 480, 302

Lallement R., Babusiaux C., Vergely J. L., Katz D., Arenou F., Valette B., Hottier C., Capitanio L., 2019, A&A, 625, A135

Littlefair S. P., Dhillon V. S., Marsh T. R., Gänsicke B. T., Southworth J., Watson C. A., 2006a, Science, 314, 1578

Littlefair S. P., Dhillon V. S., Marsh T. R., Gänsicke B. T., 2006b, MNRAS, 371, 1435

Littlefair S. P., Dhillon V. S., Marsh T. R., Gänsicke B. T., Baraffe I., Watson C. A., 2007, MNRAS, 381, 827

Littlefair S. P., Dhillon V. S., Marsh T. R., Gänsicke B. T., Southworth J., Baraffe I., Watson C. A., Copperwheat C., 2008, MNRAS, 388, 1582

Liu W., Hu J. Y., 2000, ApJS, 128, 387

Malkova A. et al., 2016, Astron. Telegram, 8956, 1

Martini P. et al., 2011, PASP, 123, 187

Mason K. O. et al., 2001, A&A, 365, L36

McAllister M. J. et al., 2017, MNRAS, 467, 1024

Merrill P. W., 1923, ApJ, 58, 215

Miller W. J., 1971, Ric. Astron., 8, 167

Morganson E. et al., 2015, ApJ, 806, 244

Morokuma T., Tominaga N., Matsumoto E., Shibata T., Yamanaka M., Tanaka M., 2014, Cent. Bur. Electron. Telegrams, 4013, 1

Morrissey P. et al., 2007, ApJS, 173, 682

Mowlavi N. et al., 2021, A&A, 648, A44

Mukadam A. S., Gänsicke B. T., Szkody P., Aungwerojwit A., Howell S. B., Fraser O. J., Silvestri N. M., 2007, ApJ, 667, 433

Munari U., Bianchini A., Claudi R., 1990, IAU Circ., 5024, 2

Munari U., Moretti S., Maitan A., 2020, A&A, 639, L10

Nakano S., Tago A., Nishiyama K., Sakamoto T., 2007, IAU Circ., 8821, 1

Nakata C. et al., 2014, PASJ, 66, 116

Nelemans G., Siess L., Repetto S., Toonen S., Phinney E. S., 2016, ApJ, 817, 69

Newville M., Stensitzki T., Allen D. B., Rawlik M., Ingargiola A., Nelson A., 2016, Astrophysics Source Code Library, record ascl:1606.014

Oliveira A. S., Rodrigues C. V., Martins M., Palhares M. S., Silva K. M. G., Lima I. J., Jablonski F. J., 2020, AJ, 159, 114

Page M. J. et al., 2012, MNRAS, 426, 903

Pala A. F., Schmidtobreick L., Tappert C., Gänsicke B. T., Mehner A., 2018, MNRAS, 481, 2523

Pala A. F. et al., 2019, MNRAS, 483, 1080

Pala A. F. et al., 2020, MNRAS, 494, 3799

Pala A. F. et al., 2022, MNRAS, 510, 6110

Paterson K., Woudt P. A., Warner B., Breytenbach H., Gilligan C. K., Motsoaledi M., Thorstensen J. R., Worters H. L., 2019, MNRAS, 486, 2422

Patterson J., 1998, PASP, 110, 1132

Patterson J., 2011, MNRAS, 411, 2695

Patterson J. et al., 1998, PASP, 110, 1290

Patterson J., Thorstensen J. R., Kemp J., 2005, PASP, 117, 427

Pavlenko E. P., Kato T., Sosnovskij A. A., Andreev M. V., Ohshima T., Sklyanov A. S., Bikmaev I. F., Galeev A. I., 2014, PASJ, 66, 113

Peters C. S., Thorstensen J. R., 2006, PASP, 118, 687

Petit M., 1960, J. Obs., 43, 17

Poggiani R., 2009, Astron. Nachr., 330, 77

Price-Whelan A. M., Hogg D. W., Foreman-Mackey D., Rix H.-W., 2017, ApJ, 837, 20

Ramsay G. et al., 2018, A&A, 620, A141

Rappaport S., Verbunt F., Joss P. C., 1983, ApJ, 275, 713

Raymond S. N. et al., 2003, AJ, 125, 2621

Rebassa-Mansergas A., Parsons S. G., Copperwheat C. M., Justham S., Gänsicke B. T., Schreiber M. R., Marsh T. R., Dhillon V. S., 2014, ApJ, 790, 28

Richards G. T. et al., 2002, AJ, 123, 2945

Richter G. A., 1970, Zentralinstitut fuer Astrophysik Sternwarte Sonneberg Mitteilungen ueber Veraenderliche Sterne, 5, 99

Richter G. A., Notni P., Tiersch H., 1988, Astron. Nachr., 309, 91

Ricker G. R. et al., 2015, J. Astron. Telesc. Instrum. Syst., 1, 014003

Ritter H., Kolb U., 2003, A&A, 404, 301

Robertson J. W., Honeycutt R. K., Turner G. W., 1995, PASP, 107, 443

Rodriguez A. C. et al., 2023, ApJ, 945, 141

Roming P. W. A. et al., 2005, Space Sci. Rev., 120, 95

Sahman D. I., Dhillon V. S., Knigge C., Marsh T. R., 2015, MNRAS, 451, 2863

Savoury C. D. J. et al., 2011, MNRAS, 415, 2025

Schaefer B. E., 2021, Res. Notes Am. Astron. Soc., 5, 150

Schaefer B. E. et al., 2019, MNRAS, 487, 1120

Schimeczek C., Wunner G., 2014, ApJS, 212, 26

Schlafly E. F., Finkbeiner D. P., 2011, ApJ, 737, 103

Schmidt R. E., 2020, AAVSO, 48, 53

Schmidt G. D. et al., 2005a, ApJ, 620, 422

Schmidt G. D. et al., 2005b, ApJ, 630, 1037

Schmidt G. D., Szkody P., Silvestri N. M., Cushing M. C., Liebert J., Smith P. S., 2005c, ApJ, 630, L173

Schmidt G. D., Szkody P., Henden A., Anderson S. F., Lamb D. Q., Margon B., Schneider D. P., 2007, ApJ, 654, 521

Schmidt G. D., Smith P. S., Szkody P., Anderson S. F., 2008, PASP, 120, 160

Schreiber M. R. et al., 2010, A&A, 513, L7

Schreiber M. R., Zorotovic M., Wijnen T. P. G., 2016, MNRAS, 455, L16

Schreiber M. R., Belloni D., Gänsicke B. T., Parsons S. G., Zorotovic M., 2021, Nature Astron., 5, 648

Schwarzenberg-Czerny A., 1989, MNRAS, 241, 153

Shappee B. J. et al., 2013, Astron. Telegram, 5052, 1

Shears J., Pickard R., Krajci T., Poyner G., 2008, J. Br. Astron. Assoc., 118, 145

Sheets H. A., Thorstensen J. R., Peters C. J., Kapusta A. B., Taylor C. J., 2007, PASP, 119, 494

Shurpakov S. et al., 2014, Astron. Telegram, 5732, 1

Sion E. M., Godon P., 2015, Acta Polytechnica CTU Proc., 2, 35

Siviero A., Munari U., 2016, Astron. Telegram, 9862, 1

Smee S. A. et al., 2013, AJ, 146, 32

Southworth J., Gänsicke B. T., Marsh T. R., de Martino D., Hakala P., Littlefair S., Rodríguez-Gil P., Szkody P., 2006, MNRAS, 373, 687

Southworth J. et al., 2008, MNRAS, 391, 591

Southworth J., Marsh T. R., Gänsicke B. T., Steeghs D., Copperwheat C. M., 2010, A&A, 524, A86

Srivastava M. K., Ashok N. M., Banerjee D. P. K., Sand D., 2015, MNRAS, 454, 1297

Stanek K. Z. et al., 2013, Astron. Telegram, 5118, 1

Steele I. A. et al., 2004, in Oschmann J. M., Jr, ed., Proc. SPIE Conf. Ser. Vol. 5489, Ground-based Telescopes. SPIE, Bellingham, p. 679

Strauss M. A. et al., 2002, AJ, 124, 1810

Swierczynski E. et al., 2010, in Prša A., Zejda M., eds, ASP Conf. Ser. Vol. 435, Binaries – Key to Comprehension of the Universe. Astron. Soc. Pac., San Francisco, p. 297

Szkody P., 1985, AJ, 90, 1837

Szkody P., Ingram D., 1994, ApJ, 420, 830

Szkody P. et al., 2002, AJ, 123, 430

Szkody P. et al., 2003, AJ, 126, 1499

Szkody P. et al., 2004, AJ, 128, 1882

Szkody P. et al., 2005, AJ, 129, 2386

Szkody P. et al., 2006, AJ, 131, 973

Szkody P. et al., 2007, AJ, 134, 185

Szkody P. et al., 2009, AJ, 137, 4011

Szkody P. et al., 2011, AJ, 142, 181

Szkody P., Everett M. E., Dai Z., Serna-Grey D., 2018, AJ, 155, 28

Szkody P. et al., 2020, AJ, 159, 198

Tampo Y. et al., 2020, PASJ, 72, 49

Taylor C. J., Thorstensen J. R., 1996, PASP, 108, 894

Thorstensen J. R., 1997, PASP, 109, 1241

Thorstensen J. R., 2013, PASP, 125, 506

Thorstensen J. R., 2020, AJ, 160, 6

Thorstensen J. R., Halpern J. P., 2009, Astron. Telegram, 2177, 1

Thorstensen J. R., Halpern J., 2013, AJ, 146, 107

Thorstensen J. R., Skinner J. N., 2012, AJ, 144, 81

Thorstensen J. R., Taylor C. J., 1997, PASP, 109, 1359

Thorstensen J. R., Taylor C. J., Becker C. M., Remillard R. A., 1997, PASP, 109, 477

Thorstensen J. R., Fenton W. H., Patterson J., Kemp J., Halpern J., Baraffe I., 2002, PASP, 114, 1117

Thorstensen J. R., Taylor C. J., Peters C. S., Skinner J. N., Southworth J., Gänsicke B. T., 2015, AJ, 149, 128

Thorstensen J. R., Ringwald F. A., Taylor C. J., Sheets H. A., Peters C. S., Skinner J. N., Alper E. H., Weil K. E., 2017, Res. Notes Am. Astron. Soc., 1, 29

Townsley D. M., Gänsicke B. T., 2009, ApJ, 693, 1007

Uthas H., Knigge C., Long K. S., Patterson J., Thorstensen J., 2011, MNRAS, 414, L85

Vladimirov V. et al., 2017, Astron. Telegram, 10415, 1

Vogt N., Bateson F. M., 1982, A&AS, 48, 383

Warner B., 2003, Cataclysmic Variable Stars. Cambridge Univ. Press, Cambridge

Watson C. L., Henden A. A., Price A., 2006, Soc. Astron. Sci. Ann. Symp., 25, 47

Webbink R. F., Wickramasinghe D. T., 2002, MNRAS, 335, 1

Wei J., Li C., Xu D., Hu J., Li Q., 1997, Acta Astrophys. Sinica, 17, 107

Welsh B. Y. et al., 2005, AJ, 130, 825

Welzl E., 1991, in Maurer H., ed., New Results and New Trends in Computer Science. Springer, Berlin, Heidelberg, p. 359

Whyte C. A., Eggleton P. P., 1980, MNRAS, 190, 801

Williams G., 1983, ApJS, 53, 523

Wils P., Gänsicke B. T., Drake A. J., Southworth J., 2010, MNRAS, 402, 436

Wright D. et al., 2012, Astron. Telegram, 4516, 1

Yecheistov V. et al., 2013, Astron. Telegram, 5536, 1

York D. G. et al., 2000, AJ, 120, 1579

SUPPORTING INFORMATION

Supplementary data are available at *MNRAS* online.

supp_data

Please note: Oxford University Press is not responsible for the content or functionality of any supporting materials supplied by the authors. Any queries (other than missing material) should be directed to the corresponding author for the article.

APPENDIX A: TABLE OF CVS OBSERVED

Table A1. CVs from the plate survey. Distances are from Bailer-Jones et al. (2021) and variable types from Watson, Henden & Price (2006) unless indicated in blue. The references for the initial discovery, spectrum, and period (where known) are also shown. New discoveries, orbital periods, and identifications are shown in blue. Suffixes to the classifications: Tentative values.

SDSS	Name	Gaia EDR3 source_id	Period (h)	Gaia G (mag)	Distance (pc)	Variable Type	Cartons	Disc	Sp	P
J000600.15 + 012129.8		2738755406045571968	1.52(10)	19.57	352	WZ Sge:§:	gg,u2,wd	1	1	1
J003827.05 + 250925.0	1RXS J003828.7 + 250920	2806802123399581056	2.26826(2)	18.63	503	SU UMa	cv,gg,u1,u2	28	12	84
J003941.08 + 005427.5	SDSS J003941.06 + 005427.5	2543387173121121216	1.523(2)	20.76	1078	WZ Sge:	cv,u1,u2,u4	53	53	74
J004335.16-003729.7	SDSS J004335.14-003729.8	2530961280492678528	1.3721(14)	19.85	447	WZ Sge:	cv,gg,u2,wd	115	115	33
J014227.07 + 001729.8		2510205490257050496	1.88(4)	19.89	697	Polar:	cv,u1,u2	105	105	1
J015543.47 + 002807.4	FL Cet	2507796391561705728	1.452389(1)	18.65	317	Polar + E	cv,gg,u1,u2	54	54	119
J020712.72-014116.3	SDSSJ020712.71-014116.2	2494386992562185088	1.55(15)	20.27		Polar:	cv	8	8	1
J020809.57 + 565239.7		505110900157013376		18.77	2961	CV	u4	39	1	
J021008.33 + 571121.0	UV Per	4571065016771769472	1.557(3)	17.75	250	SU UMa	cv	16	16	2
J021315.48 + 533822.9	MASTER OT J021315.37 + 533822.7	4553809513090048320	2.549(7)*	20.05	3224	SU UMa	cv	63	1	71
J022102.79 + 732245.0	ASASSN-14jq	546910213373341184	1.32427(31)*	19.94	425	WZ Sge	cv,gg,wd	24	1	121
J022623.34 + 711831.5	AM Cas	545338083544363392	3.9576(3)	14.37	420	U Gem	cv,gg,u1,u2			
J023322.61 + 005059.4	HP Cet	2500552912036565120	1.601(2)	20.12	683	WZ Sge:§:	cv	54	94	94
J024131.07 + 593630.5	ASASSN-16jv	464373929923792384		19.84	607	U Gem	cv	24	1	
J040834.99 + 511448.2	FO Per	2507008531408949476	4.126(12)	16.15	587	U Gem	cv	17	97	87
J041844.44 + 510731.2	NS Per	271562333932151040	6.296(1)	17.43	1076	U Gem	cv	77	97	1
J042609.34 + 354144.5	MASTER OT J042609.34 + 354144.8	176429285061830144	1.5720(7)	16.14	184	SU UMa	cv,gg,u1,u2	37	75	41
J043127.01 + 352713.0	ASASSN-16og	174868189003974016		20.37	1677	SU UMa	cv	24	1	
J044321.37 + 472125.8	V0392 Per	254361745823908736	1.5841(4)	16.17	3453	Nova	cv	21		61
J050503.07 + 222529.8	ASASSN-15su	3418286072169340416	1.608(7)*	19.12	588	SU UMa	cv	24	1	99
J052433.47-070527.9	CSS 101108:052433-070528	3207332631484540416		20.59	1528	SU UMa:	cv	36	1	
J052834.08 + 331821.7	QZ Aur	3449050362952844288	8.579910(1)	16.87	2528	Nova	cv			42
J052859.54-033352.4	V1159 Ori	3210749947983249408	1.49272(3)	14.28	351	ER UMa	cv	51	51	69
J061204.48 + 252832.6	HQ Gem	3426743917723751680		19.31	3838	U Gem	cv		1	
J062157.13 + 404236.1	ASASSN-18bz	956899025419314816		19.9	3324	U Gem	cv	79	1	
J062406.13 + 400743.8		956670430081266176		18.54	1728	NL	u1,u2	1	1	
J062429.71 + 002105.8	ASASSN-15cu	3120280997380365824	2.429755(4)	18.86	468	SU UMa	cv	40	1	1
J062601.53-035523.0	Gaia17cdo	3116642228070616192		19.19	1184	DN	cv	111	1	
J062724.39 + 161329.6	Gaia18atj	3369335048381292032	10.428	18.15	3919	U Gem	cv		1	
J062953.89-033508.4	1RXS J062954.6-033520	3105034928633782400	9.12	13.53	652	Z Cam	cv	64	1	108
J063047.05 + 023931.2	ASASSN-16ow	3124075927403447936	2.1425(13)*	20.57	3374	SU UMa	cv	47	1	71
J063301.11 + 030334.1		3130088774241620608		18.3	242	WZ Sge:	wd	1	1	
J063304.77 + 032422.8	Gaia17ber	3130135544980839680		19.1	2548	U Gem	cv	100	1	
J063516.63 + 030313.6		3130064176963184896	1.4717(2)	18.95	643	Polar:	wd	1	1	1
J063844.17 + 181611.4	UV Gem	3371136087085232128	2.226(5)*	18.81	722	SU UMa	cv		1	96
J070533.79-125004.7		3044836838812715264		18.7	246	CV:	wd	1	1	
J070816.61-124544.8	ASASSN-16an	3044908474565329280		19.16	2071	U Gem	cv	60	1	

Table A1 – *continued*

SDSS	Name	Gaia EDR3 source_id	Period (h)	Gaia G (mag)	Distance (pc)	Variable Type	Cartons	Disc	Sp	P
J073339.29 + 212200.8	CSS 091111:073339 + 212201	865345406593708160		19.37	1961	U Gem	cv	43	43	
J073758.55 + 205544.6	SDSS J073758.55 + 205544.5	673118544624392576		19.79	974	SU UMa:	cv	13	1	
J073817.74 + 285519.7	SDSS J073817.75 + 285519.7	878597549661945984	5.555(1)	18.46	1204	U Gem + E	cv,gg,u1,u2	113	113	1
J074222.55 + 172806.7	MLS 110309:074223 + 172807	671077782322909696		20.04	1828	U Gem	cv	36	114	
J074419.74 + 325448.2	CSS 091029:074420 + 325448	881969129052843520	0.55	19.83		AM CVn	cv	36	43	95
J074859.55 + 312512.5	SDSS J074859.55 + 312512.6	880821067114616832	1.39946616(2)	18.37	542	SU UMa + E	cv,gg,u1,u2,wd	13	15	26
J074917.11 + 365427.9	SDSSJ074917.11 + 365428.0	919046658301858048	1.3401(1)	19.17	820	Polar:	cv	8	8	8
J075107.51 + 300628.3	SDSS J075107.50 + 300628.4	878968875354903040	1.3918(3)*	19.68	1366	SU UMa	cv,u1,u2,wd	13	1	67
J075233.17 + 294339.5		875941782403757056	1.4455(1)	18.5	702	DN	gg,u1,u2	98	1	1
J075240.45 + 362823.2		918840426857988736		20.0	631	Polar + E	cv	113	113	48
J075331.99 + 375800.7	CSS 100407:075332 + 375801	919213474830239616	1.5363(1)	19.21	1699	MCV:	cv,u1,u2	36	43	1
J075540.64 + 264618.1	V0516 Gem	874545471356863104	1.4883(1)	18.74	359	Polar:	cv	59	1	1
J080538.98 + 354054.9	CSS 170417:080539 + 354055	906152376204919040	5.2069(1)	20.69	1770	U Gem	cv	38	1	1
J080853.73 + 355053.6	SDSS 080416:080854 + 355053	906214223733883264		19.98	1807	U Gem	cv,u2	106	3	
J081931.24 + 213338.0	MLS 151206:081931 + 213338	676203568093232512		19.46	2768	IP:	cv,u2	110	86	
J082253.13 + 231300.6	SDSS J082253.12 + 231300.6	678153002209054336		19.8	3077	CV:	cv	45	45	
J083619.15 + 212105.2	CC Cnc	664787098343076992	1.764(12)	17.45	493	SU UMa	cv,gg,u1,u2	7	7	73
J084400.09 + 023919.2	V0495 Hya	3079207606500040320	4.9708(6)	18.42	1467	U Gem	cv,u1,u2	113	113	1
J084413.66-012807.9	CSS 090331:084414-012807	3072558340145828864		20.37	2153	AM CVn	cv,u1,u2	43	43	
J084555.06 + 033929.3	V0498 Hya	581352651334960512	1.4536(14)*	20.72	1635	WZ Sge:§:	cv	96	43	96
J085107.39 + 030834.5	CT Hya	581110831791334400	1.59612(3)*	18.54	579	SU UMa	cv	17	113	66
J090246.54-014201.9	ASASSN-15gv	5764187028557281280	2.04(10):	20.58	1734	SU UMa:	cv	24	1	1
J090344.25-013326.1		5764195103095781120		19.53	278	AM CVn	gg,u2,wd	85	1	
J090403.48 + 035501.2	SDSS J090403.48 + 035501.2	579909164365936512	1.4336(1)	19.31	295	WZ Sge:	cv,gg,u1,u2,wd	115	115	115
J091410.72 + 013732.9	ASASSN-16as	3843535378146405888	6.043(7)	17.69	1016	U Gem	cv	46	112	112
J092614.30 + 010557.4		3844016380122912640	1.4723(1)	19.47	385	Polar	gg,u1,u2,wd	6	6	1
J092620.42 + 034542.3	GUVV J092620.4 + 034541.8	3845719592354419712		19.7	933	SU UMa	cv,u1,u2	56	1	
J093205.24 + 034332.5	ASASSN-17od	3850925956004914816		17.75	633	SU UMa:	cv	24	1	
J093238.20 + 010902.5	SDSS J093238.21 + 010902.5	3841337699215167232		19.4	3145	Polar:	cv	113	113	
J104245.16 + 371819.9	SDSS J104245.15 + 371819.8	7517777469035821312	1.82(4)	19.84	507	Polar	gg,u2	8	8	1
J112332.03 + 431717.5	CSS 090602:112332 + 431717	7833809506927814912		19.65	1261	SU UMa:	cv,u1,u2	124	43	
J113122.38 + 432238.7	MR UMa	772038105376131456	1.518(3)	17.92	328	SU UMa	cv,gg,u1,u2	88	109	35
J115419.06 + 575750.8	SDSS J115419.06 + 575750.9	845441772229861760		20.42	1144	ER UMa	cv	8	8	
J121913.06 + 204937.6	SDSS J121913.04 + 204938.3	3952276665815698560	1.3018(1)	19.19	274	WZ Sge	cv,gg,u2,wd	78	78	
J122740.86 + 513924.8	GP CVn	1571176823143875864	1.510810(2)	18.74	390	SU UMa	cv,gg,u1,u2,wd	109	109	102
J130514.73 + 582856.2	SDSS J130514.73 + 582856.3	1578672472969644288		19.23	3911	DN	cv	115	115	
J133309.19 + 143706.9	SDSS J133309.19 + 143706.9	3741755132951336192	2.1148(1)	19.55	2028	Polar	cv	45	45	1
J133941.08 + 484727.6	V0355 UMa	1558322303741820928	1.3754(4)	17.37	150	WZ Sge	cv,wd	53	53	1
J134052.05 + 151340.9	CSS 100531:134052 + 151341	3742038776886730368	2.45	17.94	822	U Gem	cv,u2	23		10

Table A1 – *continued*

SDSS	Name	Gaia EDR3 source.id	Period (h)	Gaia G (mag)	Distance (pc)	Variable Type	Cartons	References Disc	Sp	P
J135218.95+280917.1	CSS 090705:135219+280917	1451958950484177280		20.1	2263	U Gem	cv	43	43	
J135642.39+613024.4	V0427 UMa	1661194359687172480		20.47	2330	SU UMa:	cv	18	1	
J142953.55+073231.3	SDSS J142953.56+073231.2	1172464842754767488		20.23	1348	U Gem	cv,u2	13	1	
J143317.77+101122.7	SDSS J143317.78+101123.3	1176468611268115200	1.30177630(5)	18.55	232	WZ Sge	cv,gg,u1,u2,wd	31	31	102
J143435.36+334050.1		1287753107989718784		20.03	363	WZ Sge:§:	u2	1	1	
J150240.90+333423.4	NZ Boo	1289860214647954816	1.413831(1)	17.26	184	SU UMa + E	cv,gg,u1,u2,wd	109	109	84
J160809.54+542131.4	ELAISN1 MOS15-02	1429001113336695168	1.4646(5)	19.43	1168	ER UMa	cv	29	1	1
J161935.78+524631.7	DDE 32	1425200578380530048	1.675066(5)	19.28	449	Polar	cv	25	25	25
J163722.21-001957.1	V2690 Oph	4383291477376259968	1.61736(3)	19.99	1254	SU UMa	cv,u2	54	54	33
J165127.25-131809.2	SSS 130510:165127-131809	4332792802397772672	1.67:	19.91		U Gem	cv	110	1	
J165244.83+333925.5	SDSS J165244.84+333925.4	1314596271336011824	14.4313(2)	20.74	3281	SU UMa	cv,u2	53	53	
J165930.37-125327.2	V0841 Oph	4333061392472253440		13.65	815	Nova	cv	70	70	80
J170515.34+724403.3	MASTER OT J170515.37+724402.5	1655084339211334016		19.41	2686	SU UMa	cv	101	1	
J171752.03-070654.2	MASTER OT J171752.02-070654.6	4360435241974939392		20.52	3089	U Gem	cv	19	1	
J172148.84-051713.2	CSS 120611:172149-051713	4362925292215906176		20.12	3942	U Gem	cv	36	1	
J172805.34+775117.4		1705302990918074880		20.62	974	WZ Sge:	u2	1	1	
J173924.38+050049.7	ASASSN-15mk	4473606466292898688		20.54		DN	cv	24	1	
J174045.86+060350.5	PBC J1740.7+0603	4485786821746343680	1.6826(50)	15.84	232	Polar:	cv	50	50	50
J174056.31+025831.6	MG1 995493	4376325246582929920	4.143(3):	17.81	928	U Gem‡	cv,gg,u1,u2	34	1	1
J174759.88+032859.7	ASASSN-15fm	4472400370757130496		20.07	957	DN	cv	30	1	
J181111.75+124301.7		4496951052360182656		19.79	689	SU UMa:	wd	1	1	
J182122.51+614855.2	ASASSN-13at	2159834324676298880	1.901(5)	19.46	764	SU UMa	cv,gg,u1,u2	118	32	32
J182138.61+615904.0	ASASSN-14gg	2159842815827966720	1.44(3)*	19.78	722	SU UMa	cv,wd	68	1	117
J182205.84+270849.8	MASTER OT J182205.85+270849.7	4585224931075337216		20.66	1772	SU UMa	cv	91	1	
J182643.55+613816.5	MGAB-V733	2159773512236202624	2.0654	20.62	2118	SU UMa	cv	11	1	1
J183052.72+265514.9		4585376839774011520		18.79	1175	SU UMa	u2	9	1	
J183211.36+615505.9	ASASSN-13ah	2159698023890909184	1.5874(3)*	20.47	960	SU UMa	cv	89	1	99
J192914.75+202759.5	NQ Vul	2017742684676480896	3.516(2)	17.29	1170	Nova	cv	83	83	65
J192927.83+202035.0	1RXS J192926.6+202038	2017736641707652608	3.89(3)	17.58	567	U Gem	cv	120	112	112
J195837.08+164128.4	AW Sge	1820137772050526464	1.788(5)*	19.29	604	SU UMa	cv	58	1	123
J200318.50+170251.4	RZ Sge	1820209309009288960	1.63872	18.29		SU UMa	cv	58	58	14
J200611.52+334237.6	V1363 Cyg	2058291887543939968	2.42(14):	16.28	1641	U Gem	cv	82	116	27
J200934.41+550525.7		2185841249306525696		16.52	1707	NL	gg	49	1	
J202812.47+414836.3	V2467 Cyg	2060808097698964768	3.83	18.04	1847	IP:	cv	20	76	
J204638.68+603803.0	V0713 Cep	2194206707428148480	2.0500424(1)	18.35	319	SU UMa + E	cv	52	1	57

Table A1 – *continued*

SDSS	Name	Gaia EDR3 source_id	Period (h)	Gaia G (mag)	Distance (pc)	Variable Type	Cartons	Disc	Sp	P
J205423.76+601706.7	V0962 Cep	2194035971882977728		19.28	3095	Nova	cv	103	1	
J212654.54-012054.3	CRTS J212654.5-012054	2686013551247649152		19.06	1676	Polar	cv,u2	36	36	
J213432.34-012040.5	CSS 081120:213432-012040	2686614060690086016		18.59		U Gem	cv	36	1	
J221827.75+192520.2	Swift J2218.5+1925	1777232423131443840	2.159(24)	17.31	240	Polar	cv,gg,u1,u2	22	62	62
J221900.24+201831.2	SDSS J221900.24+201831.1	1778468682222798080	3.36(1)	18.23	821	DN	gg,u1,u2	8	8	8
J222117.33+194817.6	ASASSN-19wi	1777640754262037248		18.77	708	DN	gg,u1,u2	24	1	
J234440.54-001206.1	MLS 100904:234441-001206	2642699218384434432	1.84111(7)*	20.07	668	SU UMa	cv,u2	110	43	66

Notes. Cartons: cv mwm_cb_cvcandidates, gg mwm_cb_gaiagalex, u1 mwm_cb_uvex1, u2 mwm_cb_uvex2, u4 mwm_cb_uvex4, wd mwm_wd
References: (1) This work, (2) Thorstensen & Taylor (1997), (3) Wright et al. (2012), (4) Richter, Notni & Tiersch (1988), (5) Thorstensen (2013), (6) Rodriguez et al. (2023), (7) Munari, Bianchini & Claudi (1990), (8) Inight et al. (2023), (9) MGAB Variable Star Catalog, (10) Gänsicke et al. (2006), (11) Malkova et al. (2016), (12) Szkody et al. (2018), (13) Wils et al. (2010), (14) Kato et al. (2014b), (15) Lamost 8/1/2016, (16) Szkody (1985), (17) Petit (1960), (18) Stanek et al. (2013), (19) Vladimirov et al. (2017), (20) Nakano et al. (2007), (21) Richter (1970), (22) Thorstensen & Halpern (2009), (23) Thorstensen & Skinner (2012), (24) ASAS-SN CV candidate, (25) Denisenko & Martinelli (2016), (26) vsnet 19297, (27) vsnet 13294, (28) VSNET 12318, (29) Gezari et al. (2013), (30) Paterson et al. (2019), (31) Szkody et al. (2007), (32) Thorstensen (2020), (33) Southworth et al. (2008), (34) Kraus et al. (2007), (35) Thorstensen et al. (2015), (36) Drake et al. (2014), (37) Denisenko et al. (2012), (38) Hodgkin et al. (2020), (39) Mowlavi et al. (2021), (40) Delgado et al. (2017b), (41) Kato et al. (2014a), (42) Schaefer et al. (2019), (43) Breedt et al. (2014), (45) Szkody et al. (2009), (46) VSNET 19440, (47) Siviero & Munari (2016), (48) Homer et al. (2005), (49) Heinze et al. (2018), (50) Halpern & Thorstensen (2015), (51) Jablonski & Cieslinski (1992), (52) Antipin & Kroll (2003), (53) Szkody et al. (2005), (54) Szkody et al. (2002), (55) Bruch, Fischer & Wilmsen (1987), (56) Welsh et al. (2005), (57) Boyd et al. (2011), (58) Vogt & Bateson (1982), (59) Morokuma et al. (2014), (60) Delgado et al. (2019), (61) Schmidt (2020), (62) Thorstensen & Halpern (2013), (63) Yecheistov et al. (2013), (64) Ritter & Kolb (2003), (65) Schaefer (2021), (66) Kato et al. (2010), (67) vsnet 15408, (68) Delgado et al. (2018a), (69) Thorstensen et al. (1997), (70) Williams (1983), (71) Kato et al. (2017), (72) Chen et al. (2020), (73) Thorstensen (1997), (74) Southworth et al. (2010), (75) Hou et al. (2020), (76) Poggiani (2009), (77) Hoffmeister (1966), (78) Szkody et al. (2011), (79) Jayasinghe et al. (2018), (80) Peters & Thorstensen (2006), (81) Swierczynski et al. (2010), (82) Miller (1971), (83) Cordoni, Gleizes & Jasniewicz (1977), (84) Inight et al in prep, (85) Carter et al. (2013), (86) Szkody et al. (2020), (87) Sheets et al. (2007), (88) Wei et al. (1997), (89) Shappee et al. (2013), (90) Liu & Hu (2000), (91) Denisenko et al. (2014), (92) Szkody & Ingram (1994), (93) Delgado et al. (2017a), (94) Southworth et al. (2006), (95) Ramsay et al. (2018), (96) Kato et al. (2009), (97) Bruch (1989), (98) VSNET 7967, (99) Kato et al. (2016), (100) Delgado et al. (2009a), (101) Balanutsa et al. (2013), (102) Littlefair et al. (2008), (103) Srivastava et al. (2015), (104) Campbell & Shafter (1995), (105) Carbon, Henze & Nelson (2017), (106) Drake et al. (2009a), (107) Fremling et al. (2018), (108) Arjyotha et al. (2009), (109) Szkody et al. (2006), (110) CRTS candidate CV, (111) Delgado et al. (2017c), (112) Thorstensen et al. (2017), (113) Szkody et al. (2003), (114) Oliveira et al. (2020), (115) Szkody et al. (2004), (116) Bruch & Schimpke (1992), (117) vsnet 20079, (118) Garnavich & Deal (2013), (119) Schmidt et al. (2005a), (120) Denisenko & Sokolovsky (2011), (121) Kato et al. (2015), (122) Taylor & Thorstensen (1996), (123) Shears et al. (2008), and (124) Drake et al. (2009b).

*Superhump periods.
†Low accretion SU UMa.
‡CVs with unusual state changes.
§Period bouncers.
+E Eclipsing.

APPENDIX B: SPECTRAL CONFIRMATION OF PREVIOUSLY KNOWN SYSTEMS

The spectra and light curves of the following objects are shown in the supplementary material. We note below any new information; we have not commented on well-studied systems where we have nothing new to add.

B1 J0213 + 5338

The spectrum shows Balmer emission lines. Together with the frequent outbursts and superoutbursts in the ZTF light curve, this is consistent with the previous classification of SU UMa and a period of 2.549 h.

B2 J0221 + 7322

The white dwarf is visible in the spectrum and there is a double peaked Hα line. This combination is confirmation of the WZ Sge classification.

B3 J0241 + 5936

The spectrum is reddened by 0.39 mag due to being in the Galactic plane. It shows Balmer emission lines. There is an outburst in the ZTF light curve, and this, together with its position in the HR diagram, confirms that this is a U Gem.

B4 J0431 + 3527

Although the spectrum of this object has a relatively low SNR, it reveals a strong double-peaked Hα emission line. There are four outbursts apparent in the ZTF light curve including at least one superoutburst – confirming the existing classification of SU UMa.

B5 J0505 + 2225

The spectrum shows Balmer and He I emission lines. The ZTF light curve shows dwarf nova outbursts confirming the previous classification of SU UMa.

B6 J0524–0705

Despite poor flux calibration, the Balmer, He II, and He I emission lines are visible in the spectrum. The ZTF light curve shows seven outbursts, two of which appear to be superoutbursts with superhumps visible. We classify this as a probable SU UMa.

B7 J0612 + 2528

This is HQ Gem and is positioned on the edge of the main sequence in the HR diagram. The spectrum shows Balmer and He I emission lines. The light curve shows multiple outbursts, confirming that this is a U Gem.

B8 J0621 + 4042

This is positioned on the edge of the main sequence in the HR diagram. Lines from the donor are visible in the spectrum as well as Balmer emission lines, which confirm the classification of U Gem.
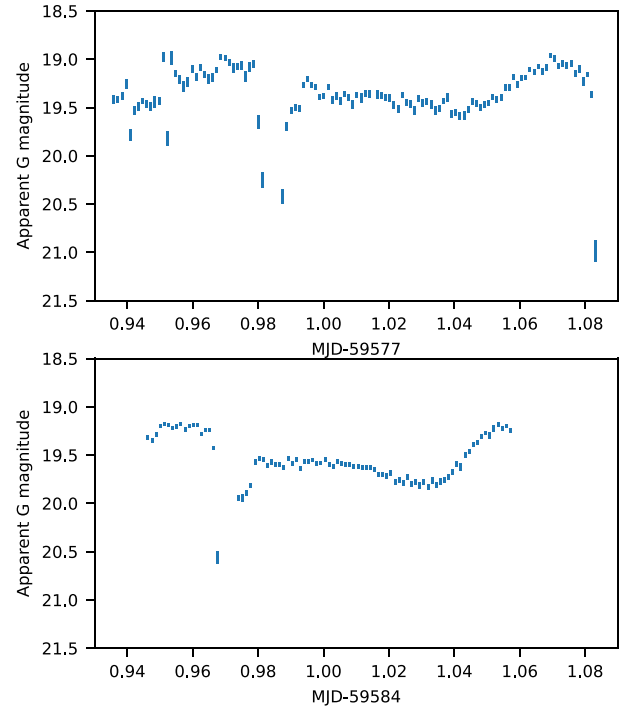
Figure B1. Photometric observations of J0624 + 0021 using the Liverpool Telescope. Top panel: 2021 December 02 showing a clear eclipse and the start of a second. Bottom panel: 2022 January 05 showing a single eclipse.
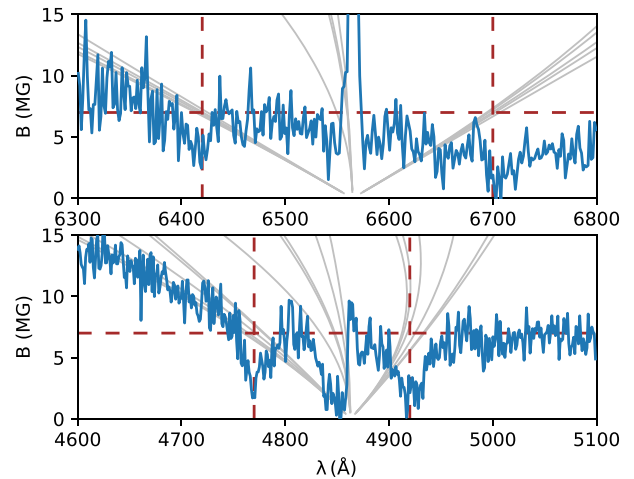
Figure B2. Spectra of Hα and Hβ lines of J0755 + 2646 showing the Zeeman splitting lines (Schimeczek & Wunner 2014). The lines coincide with absorption lines for a magnetic field of $B \simeq 7$ MG.

B9 J0624 + 0021

We obtained photometric light curves (Fig. B1), which show a deep eclipse. These curves were combined with ZTF data to determine the correct alias resulting in the ephemeris HJD($\phi = 0$) $2\,459\,578.48972(7) + N \times 0.101240(1)$. Lines from the donor are visible in the spectrum, along with Balmer emission lines from the accretion disc. The ZTF light curves show outbursts and at least one superoutburst, causing us to classify this as an SU UMa in the period gap.

B10 J0626−0355

The spectrum shows Balmer, He II and He I emission lines, which, together with the outbursts in the ZTF light curves, confirm the classification as a dwarf nova.

B11 J0629−0335

The spectrum shows Balmer emission lines albeit with poor calibration, which confirms the classification in Arjyotha et al. (2009) of a Z Cam.

B12 J0630 + 0239

The spectrum shows single-peaked Balmer emission lines as well as absorption lines from the donor although the flux calibration is poor. These characteristics are consistent with the classification of Kato et al. (2017) that this is a low-inclination SU UMa.

B13 J0633 + 0324

Double-peaked Balmer emission lines from an accretion disc as well as absorption lines from the donor are visible in the spectrum. It is very close to the main sequence in the HR diagram, and the SED indicates a mid-K type donor. The donor characteristics, together with the outbursts visible in the ZTF light curves, lead us to the classification of U Gem.

B14 J0708−1245

This is ASASSN-16an. It is close to the galactic plane ($b = -2.1$) and significantly reddened with $E(B - V) \simeq 0.7$. The spectrum shows Balmer and He I emission lines together with absorption lines from the donor. The ZTF light curve shows multiple outbursts. Taken together, this confirms the U Gem classification.

B15 J0737 + 2055

The spectrum shows narrow Balmer and He I emission lines, indicating a low inclination system. There is a single five-magnitude outburst in the ZTF light curve; however, there are too few data points to confirm whether or not this is a superoutburst. It is closer to the white dwarf cooling sequence than the main sequence in the HR diagram. This is probably an SU UMa.

B16 0751 + 3006

The spectrum shows strong Balmer and He I emission lines. The spectrum together with the light-curve outbursts and known period of 1.3918 h confirm the SU UMa classification.

B17 J0752 + 2943

The spectrum shows Balmer and He I emission lines and also emission of He II at 4686 Å. The CRTS light curve shows a ∼3 magnitude variation over a 5-yr period with a 1.5 magnitude outburst on MJD = 55 211 while the ZTF light curve shows a 1.5 mag outburst on MJD = 58 511. Curiously, the long-term light curve shows a smooth change not typical of a high-low switch. We checked nearby objects in CRTS, and they did not show this type of variation. There is ellipsoidal modulation in the ZTF light curve at a period of 1.1445(7) h implying an orbital period of 2.289(2) h. Together with the outbursts, this confirms the classification of a dwarf nova.

B18 J0753 + 2943

The spectrum shows strong Balmer and He I emission lines and J0753 + 2943 is located between the main sequence and the white dwarf cooling sequence in the HR diagram. There are two outbursts visible in the ZTF light curve. A periodogram of the ZTF light curve shows a reliable period of 1.4455(1) h.

B19 J0755 + 2646

We have 25 radial velocity measurements with moderate SNR over five epochs spanning 86 d. We find a period of 1.4883(1) h. The spectrum shows Zeeman splitting around weak Hα, Hβ, and Hγ lines (see Fig. B2). This is therefore a magnetic white dwarf and not a U Gem dwarf nova; the field strength of $B \simeq 7$ MG suggests an intermediate polar although polars can have magnetic fields as weak as this (Ferrario et al. 1995). There is slight contamination in the spectrum from a background galaxy. It is currently in a low state (*Gaia* EDR3 $m_G = 18.74$), but previously, it has been in a high state (Pan-STARRS $m_g = 16.6$ and *Gaia* DR2 $m_G = 16.82$). The transient reported by Morokuma et al. (2014) is the same magnitude as the high states reported by Pan-STARRS and *Gaia* DR2. The magnitude reported by *Gaia* DR2 is based on 160 observations, which would suggest a prolonged high state rather than transient behaviour. This system might also be a low accretion rate polar with the white dwarf accreting material from the donor's wind rather than Roche-lobe overflow (Breedt et al. 2012). We tentatively classify this as a polar.

B20 J0805 + 3540

The spectrum shows Balmer, He II and He I emission lines. The spectrum has the appearance of a K-star while an absorption dip just over 5000 Å is reminiscent of QZ Per (Thorstensen et al. 2002). A periodogram of the ZTF light curve shows ellipsoidal modulation with an orbital period of 5.2 h. This is a U Gem and may have an evolved donor.

B21 J0902−0142

The spectrum shows double peaked Balmer and He I emission lines. There are hints of TiO absorption lines from the donor − consistent with the SED. We have a tentative period from the radial velocities of 2.04(10) h. The ZTF light curve shows outbursts; taken together with the tentative period this is probably an SU UMa.

B22 J0903−0133

The spectrum shows strong Helium emission and no hydrogen lines. This confirms that this object is an AM CVn as suggested by Carter et al. (2014).

B23 J0926 + 0345

J0926 + 0345 was in outburst during one of the spectra (see Fig. 13 in the supplementary material). The quiescent spectrum shows strong Balmer and He I emission lines. The ZTF light curve shows numerous outbursts and at least one superoutburst. It is nearer the white dwarf cooling sequence than the main sequence in the HR diagram. We therefore classify this as an SU UMa.

B24 J0932 + 0343

The spectrum shows strong Balmer and He I emission lines. TiO and Na absorption lines from the donor are visible and also absorption lines from the white dwarf, indicating a low accretion rate. The ZTF light curve shows frequent outbursts with the hint of a superoutburst. This is probably an SU UMa.

B25 J1356 + 6130

The spectrum shows weak double peaked Balmer and He I emission lines. The white dwarf and the donor are both visible in the spectrum, indicating a low accretion rate. The photometry is dominated in the red by the bright donor. The ZTF light curve shows six outbursts including a superoutburst. This confirms that this is an SU UMa.

B26 J1429 + 0732

The spectrum shows double peaked Balmer and He I emission lines. The donor is very visible. The ZTF light curve shows 10 outbursts consistent with the classification of U Gem.

B27 J1608 + 5421

We have 12 usable radial velocities in three epochs. The tallest peak in the THE JOKER periodogram is at $\simeq 1.4646$ h and the amplitude of the periodogram falls off sharply after the two adjacent aliases. The ZTF light curve shows at least 10 outbursts (actually probably superoutbursts) with a quiescent magnitude $m \simeq 22.5$. Analysis of the light curve between 19 and 20 magnitude and $58\,376 < \text{MJD} < 58\,390$ shows superhumps with a period of $\simeq 1.506$ h, which confirms that $\simeq 1.4646$ h is the correct alias. We therefore estimate the period to be 1.4646(5) h. The frequent superhumps in the light curve suggest that this is an ER UMa type system (Robertson, Honeycutt & Turner 1995; Kato et al. 2013) – a sub-type of SU UMa.

B28 J1651–1318

Balmer emission lines are visible despite poor SNR and flux calibration. The ZTF light curve shows four outbursts while the quiescent magnitude is at least 21 and so the *Gaia* and Pan-STARRS magnitudes (19.9 and 19.5, respectively) are based on the magnitude of the outbursts. The outbursts and emission lines confirm the classification of U Gem.

B29 J1705 + 7244

The spectrum shows strong Balmer and He I emission lines with neither the donor nor the white dwarf visible. The ZTF light curve shows frequent outbursts and at least two superoutbursts. We therefore classify this as an SU UMa.

B30 J1717–0706

The spectrum shows Balmer and He I emission lines with neither the donor nor the white dwarf visible. It is next to the main sequence on the HR diagram and the donor is clearly visible in the SED. It is very faint – *Gaia* DR3 reports $m_G = 20.52$. There is no ZTF data although the CRTS data show two outbursts reaching $m \simeq 16.5$. The emission lines and outbursts confirm that this is a U Gem.
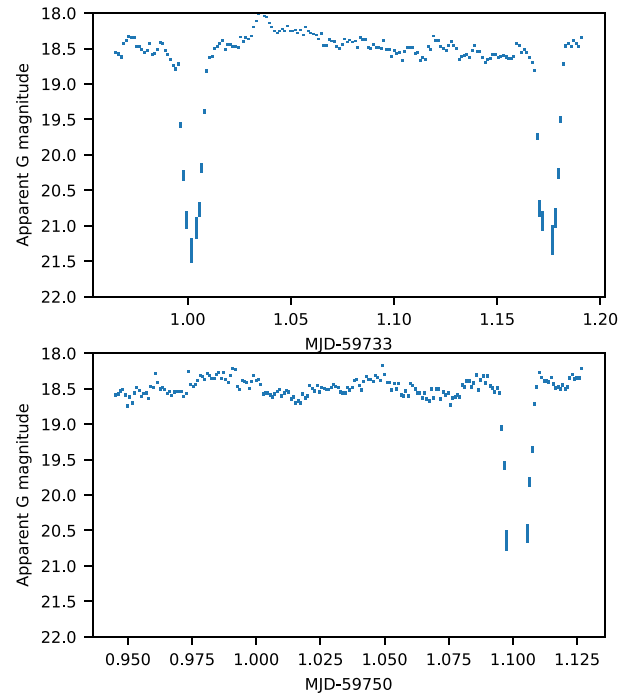
Figure B3. Photometric observations of J1740 + 0258 using the Liverpool Telescope. Top panel: 2022 June 03 showing two clear eclipses. Bottom panel: 2022 June 20 showing a single eclipse.

B31 J1721–0517

The spectrum shows strong Balmer, Paschen and He I emission lines with a very red continuum from the donor. It is close to the main sequence in the HR diagram. The ZTF light curve shows three outbursts of $\Delta m \simeq 4.5$. We therefore confirm that it is a U Gem.

B32 J1739 + 0500

The spectrum shows Balmer and He I emission lines with neither the donor nor the white dwarf visible. The system is faint ($m_G = 20.48$), and the spectrum has a poor SNR. The ZTF light curves show three outbursts, and we conclude that this is a dwarf nova.

B33 J1740 + 0258

The spectrum shows Balmer and He I emission lines. TiO and Na 8194 Å absorption lines from the donor are visible. The ZTF light curve showed two outbursts with unusual state changes and J1740 + 0258 also appeared to be eclipsing. We therefore obtained LT photometry (see Fig. B3), which confirmed that J1740 + 0258 was eclipsing with ephemeris HJD($\phi = 0$)2 459 734.5074(2) $+ N \times$ 0.172724(2). This is therefore a U Gem.

B34 J1747 + 0328

The spectrum shows a CV in outburst with a synthetic magnitude $m_G = 17.5$ consistent with the outbursts in the ZTF light curve. This confirms the classification of dwarf nova.

B35 J1821 + 6159

The spectrum shows strong Balmer, Paschen, and He I emission lines with neither the donor nor the white dwarf visible. The ZTF light curve shows seven outbursts consistent with the published classification of SU UMa and superhump period of 1.44 h.

B36 J1822 + 2708

The spectrum shows strong double-peaked Balmer, Paschen, He I and Ca emission lines. It is midway between the main sequence and the white dwarf cooling sequence in the HR diagram. The ZTF light curve shows three outbursts, including a superoutburst. This is an SU UMa.

B37 J1826 + 6138

The spectrum shows weak double-peaked Balmer emission lines. The ZTF light curve shows frequent outbursts and also five super-outbursts, leading to a classification of SU UMa. We find a period of 2.0654 h from the ZTF periodogram.

B38 J1830 + 2655

We have both outburst and quiescent spectra (see Fig. 13 in the supplementary material). The quiescent spectrum shows strong Balmer, Paschen, and He I emission lines with neither the donor nor the white dwarf visible. The ZTF light curve shows frequent short outbursts and at least one superoutburst resulting in our classification of SU UMa. The light curve is unusual as the quiescent magnitude appears to fall by over a magnitude between MJD = 58800 and MJD = 59000.

B39 J1958 + 1641

The spectrum shows double-peaked Balmer emission lines. The ZTF light curve shows seven outbursts including at least one superout-burst. A periodogram of the ZTF light curve yields an orbital period of 1.723023(5) h, which is consistent with the published superhump period of 1.735(16) h.

B40 J2009 + 5505

The spectrum appears to be either that of a novalike or a dwarf nova in outburst. However the light curve shows no signs of an outburst and its position in the *Gaia* HR diagram is consistent with a novalike. This object was classified as a subdwarf in Geier et al. (2017) however the spectrum shows Hα and Hβ emission lines and that, together with the position on the HR diagram leads us to classify it as a novalike. The light curve also shows an unusual long term trend of increasing magnitude.

B41 J2054 + 6017

This is a classical nova that erupted in 2014 (Srivastava et al. 2015). It is now very faint (synthetic magnitude $m_G = 20.6$) leading to the poor SNR in the spectrum, inconsistent with the *Gaia* magnitude ($m_G = 19.3$).

B42 J2134–0120

This system was identified as a transient by CRTS (CSS 081120:213432 − 012040) and is classified as a U Gem by VSX.

Drake et al. (2014) considered it a CV based on its CRTS light curve and photometry, however, Coppejans et al. (2016) decided against a dwarf nova classification based on the same CRTS light curve. The archival photometry available shows large-amplitude ($\simeq 2$ mag) variability on time scales of months to years, with no clear periodicity. When non-detections are accounted for the ZTF photometry appears to show the outbursts of a dwarf nova. The system is very blue and also varies in the far-ultraviolet, with three separate *GALEX* detections ($m_{FUV} =$ 18.6, 20.0, and 23.5). The SDSS-V spectrum reveals a blue continuum with weak Balmer absorption lines, and no noticeable emission lines. The spectrum was obtained close to peak brightness and is consistent with a dwarf nova in outburst. *Gaia* has not obtained a parallax for this object and hence we cannot position it on the HR diagram. We therefore classify it as a U Gem.

B43 J2221 + 1948

The spectrum shows strong Balmer, Paschen, Ca (H and K) and He I emission lines with neither the donor nor the white dwarf visible. The ZTF light curve does not show outbursts and the CRTS light curve shows only one outburst from which we make a classification of dwarf nova.

APPENDIX C: WELL-KNOWN SYSTEMS

The following well-studied systems have previously published spectra. We include their spectra and light curves in the supplementary material and note below any new information.

C1 J0142 + 0017

We obtained 16 high SNR radial velocities over 3 epochs. The sine fit yielded an estimated period of 1.8777(1) h while THE JOKER identified 1.914 h. We therefore estimate the period as 1.88(4) h. This is consistent with the previous classification of a polar.

C2 J0155 + 0028

This is FL Cet − a known eclipsing polar. This spectrum is that of a polar in a low state exhibiting cyclotron humps and Zeeman splitting. It contrasts with a previous SDSS spectrum (Szkody et al. 2002) when it was in a high state.

C3 J0207–0141

We obtained 18 high SNR radial velocities over 3 epochs. A sine fit yields an estimated period of 1.5515(1) h. THE JOKER identified 1.400 h. We therefore estimate the period as 1.55(15) h. The spectrum shows strong Balmer, He II and He I emission lines consistent with the previous classification of a polar.

C4 J0233 + 0050

The spectrum and ZTF light curve confirm the previous classification of WZ Sge. However, the long period (1.6 h) and absence of the donor in the spectrum and SED indicate that this is probably a period bouncer.

C5 J0418 + 5107

Our MDM campaign on this object started with the modular spectrograph in 2018 November, and continued with the Ohio State

Multi-Object Spectrometer (OSMOS; Martini et al. 2011) in 2018 December and 2019 January. We obtained 40 usable velocities of Hα emission; the spectrum also showed a contribution from a late-type secondary; and in 33 spectra, we were able to measure usable absorption-line velocities by cross-correlating portions of the spectrum with a zero-velocity late-type template spectrum. The periods from the emission velocities and absorption velocities agreed within the uncertainties, with a weighted mean of 6.296(1) h. This is consistent with the U Gem classification − a long period with frequent outbursts. There is some reddening due to its proximity to the Galactic Plane.

C6 J0426 + 3541

Our spectrum shows double peaked Balmer and He I emission lines. The ZTF light curve shows outbursts and, intriguingly, variations in the quiescent level. It is a non-magnetic system with high inclination consistent with the previous SU UMa classification.

C7 J0443 + 4721

This is an old nova that erupted in 2018 whose decline can be seen in the ZTF light curve. Comparing the spectrum with the SED shows that J0443 + 4721 is still in a high state compared with its historical luminosity. It has an unusually long period of 3.4118 d (Munari, Moretti & Maitan 2020).

C8 J0627 + 1613

J0627 + 1613 was initially identified from a transient by Gaia Alerts (Delgado et al. 2018b). ZTF light curves show two transients $\Delta m \sim 2$ each with a duration of $\simeq 15$ d. Unusually, J0627 + 1613 is positioned slightly above the main sequence in the HR diagram. The SED is essentially a blackbody with a surface temperature $\simeq 3000$ K. The spectrum is consistent with this and suggests that this is a CV with a $\sim$ K0 donor that would explain the position in the HR diagram. We confirmed that the orbital period, estimated using the ZTF photometry by Chen et al. (2020), to be 10.428 h, is correct. This period is also consistent with a CV having a high-mass donor at an early stage in its evolution.

C9 J0738 + 2855

The spectrum shows Balmer and He I emission lines together with absorption lines from the donor. The ZTF light curve suggests that it is eclipsing; there are also at least seven outbursts. Szkody et al. (2003) found a period of 2.1 h, which is not consistent with the donor presence in the spectrum – a short period system would have a dim donor. The ZTF periodogram shows a period of 5.555(1) h. The *TESS* periodogram shows a period of 5.55(2) h.

C10 J0753 + 3758

The spectrum shows strong Balmer, He II and He I lines. The ZTF light curve shows variability but no outbursts. We have 21 radial velocities with high SNR over four epochs spanning 84 d from which we find a period of 1.5363(1) h. This period is consistent with THE JOKER. This is probably a magnetic CV as previously reported.

C11 J0805 + 3540

There are three spectra; two in a quiescent state and one during outburst. The outburst state (shown in Fig. 5 in the supplementary material) differs from the quiescent spectra by having a very strong He II emission line. There is the suspicion of TiO absorption lines from the M-dwarf in the quiescent spectra. It is located towards the white dwarf sequence in the HR diagram. The ZTF light curves show outbursts and we derive a period of 5.2069(2) h from a ZTF periodogram.. This is a U Gem and likely to have an evolved donor which would explain the helium emission and the short period for a relatively high mass donor.

C12 J0808 + 3550

We have two spectra, one in quiescence and one in outburst (see Fig. 13 in the supplementary material). The previously published spectrum (Wright et al. 2012) was taken during an outburst. Our quiescent spectrum has strong double-peaked Balmer and He I emission lines. There are frequent outbursts visible in the ZTF light curves all consistent with the dwarf nova classification.

C13 J0819 + 2133

The spectrum shows strong Balmer and He I emission lines and also TiO absorption lines from the donor. However, the unusually variable ZTF light curve shows apparent changes in state over a period of $\sim$1 y, indicating a potentially magnetic system. The synthetic magnitude of our spectrum is 21.5 and so our observation was taken during a low state. This is probably an intermediate polar.

C14 J0822 + 2313

This was identified by Szkody et al. (2009) as a CV based on a strong, broad Hα emission line in five exposures taken between 2004 November 05 and 2004 November 08. We have 29 exposures taken between 2020 November 11 and 2021 March 08, which show an M-dwarf profile but no sign of Hα emission. There are no ultraviolet or X-ray observations shown in Vizier nor evidence of outbursts in ZTF (although CRTS shows some transients). In the absence of other evidence, we can only consider this to be a Candidate CV.

C15 J0836 + 2121

This is CC Cnc that has a known period of 1.764(12) h and is in the Ritter & Kolb catalog (Ritter & Kolb 2003). The ZTF light curve not only shows short outbursts but also apparent changes of state of magnitude $\Delta m \simeq 1.5$.

C16 J0844 + 0239

This is V495 Hya. We measured a period using radial velocities of 4.9708(6) h, which is consistent with, and improves upon, the period of 4.968(17) h reported by Thorstensen et al. (2015).

C17 J0845 + 0339

This is V498 Hya. The spectrum shows double peaked Balmer emission lines. There are clear absorption lines from the white dwarf but no evidence of the donor. Assuming the Bailer-Jones et al. (2021), distance of 1635 pc is correct then V498 Hya is located above the white dwarf cooling sequence on the HR diagram;

however, this distance is not consistent with the parallax nor the earlier Bailer-Jones et al. (2018) estimate of 302 pc both of which would place V498 HYa on the white dwarf cooling sequence. The period is 1.4256 h from Kato et al. (2009) based on a seven magnitude superoutburst in 2008 January. The ZTF light curves do not show any outbursts. From the size of the 2008 outburst and the absence of subsequent observed outbursts, we conclude that it is probably a WZ Sge and also a period bouncer.

C18 J0851 + 0308

This is a well-studied system called CT Hya. In passing, we note that the ZTF light curve shows an apparent brightening over a period of $\simeq 1$ yr of $\Delta m \simeq 0.5$.

C19 J0926 + 0105

In addition to asymmetric Balmer and He I emission lines, the SDSS spectrum contains He II at 4686 Å. Both the donor and the white dwarf are visible in the form of broad Balmer absorption lines and an upturn at the red end of the SDSS spectrum, respectively. Currently, *Gaia* EDR3 has $m_G = 19.4$; however, the SED plot shows a sequence of detections several magnitudes brighter, suggesting that there has been a state change at some point. The ZTF light curve shows considerable variability, and from it, we obtain a period that is consistent with our spectroscopic period of 1.47234(1) h. This is more accurate than the period of 1.48 h reported by Rodriguez et al. (2023).

C20 J0932 + 0109

This is a bright, distant (3145 pc) object that was identified as a novalike or potential polar in Szkody et al. (2003). The spectrum shows strong Balmer, He II and He I emission lines. The emission limes are asymmetric, which, together with the He II, are consistent with being a polar. The ZTF data show variations of $\Delta m \sim 1$ over a 6-min interval that we presume is due to cyclotron beaming. We therefore classify this as a polar.

C21 J1042 + 3718

The spectrum shows distinct signs of cyclotron humps consistent with the previous classification of a polar. We have five high SNR radial velocities in one epoch. We estimate the period to be 1.82(4) h, which is consistent with THE JOKER.

C22 J1123 + 4317

Breedt et al. (2014) obtained a spectrum and classified this as a dwarf nova. Our ZTF light curve shows a single superoutburst with clearly visible superhumps. We therefore classify this as an SU UMa.

C23 J1219 + 2049

We have 10 moderate SNR radial velocities in three epochs and estimate the period to be 1.3018(1) h. The white dwarf absorption lines are clearly visible in the spectrum implying that this is a low accretion rate CV – consistent with a short period. It is located in the white dwarf cooling sequence in the HR diagram and taking account of the period and low accretion rate we classify this as a WZ Sge.

C24 J1333 + 1437

We have 13 RV data points in 3 epochs. We have improved upon the period of 2.2 ± 0.1 h from Schmidt et al. (2008). Our best fit is 2.1148(1) h, which is consistent with the earlier observation and takes advantage of the longer baseline (59 d) of our observations. It is also consistent with a periodogram from the ZTF light curve. The spectrum shows strong Balmer, He II and He I emission lines. The ZTF light curve, though sparse, shows evidence of a low state of $m \sim 21$ and a high state of $m \sim 20$. This, together with the He II emission lines, are confirmation of the previous classification of a polar.

C25 J1652 + 3339

The spectrum shows strong double-peaked Balmer and He I emission lines with both the donor and the white dwarf visible. The ZTF and CRTS light curves show frequent outbursts and at least two superoutbursts. Analysing the radial velocities using THE JOKER suggests that the orbital period may be $\simeq 1.67$ h. This is an SU UMa.

C26 J1740 + 0258

We obtained a period of 4.143(3) h from LT photometry (Fig. B3). The ZTF light curve also shows a significant state change reminiscent of the unusual CVs identified by Inight et al. (2023).

C27 J1740 + 0603

The spectrum shows strong Balmer, Paschen, He II and He I emission lines with neither the donor nor the white dwarf visible. The emission lines are asymmetric and, combined with the He II emission lines, cause us to classify this a probable polar.

C28 J2006 + 3342

The ZTF light curve shows two 'outbursts' with very long (months) decay times. Sahman et al. (2015) report that this CV is surrounded by a faint nova shell that may account for this unusual behaviour.

C29 J2126–0120

The quiescent spectrum shows strong Balmer, Paschen, He II, and He I emission lines with the donor but not the white dwarf visible. The emission lines appear to be asymmetric, and there are cyclotron humps and these, together with the He II emission, imply that this is magnetic, and we therefore classify this as a polar.

C30 J2219 + 2018

The spectrum shows strong Balmer, Paschen, He II, and He I emission lines with the donor but not the white dwarf visible. The ZTF light curve shows frequent outbursts together with an apparent standstill between MJD $\simeq 58\,970$ and MJD $\simeq 59\,250$. We therefore classify this as a dwarf nova.

APPENDIX D: UNUSABLE OBSERVATIONS

Table D1. The 12 CVs and CV candidates listed below were observed by SDSS-V; however, the quality of their spectra was too low to draw any conclusions.

SDSS name	Alternative name
SDSS J021229.78 + 570519.4	UW Per
SDSS J062632.18 + 161622.9	Gaia17cxa
SDSS J074121.62 + 313821.0	ASASSN-15dx
SDSS J074813.35 + 290512.0	V434 Gem
SDSS J085228.73 + 020102.5	CSS 160419:085229 + 020103
SDSS J142936.25 + 322629.2	CSS 140607:142936 + 322630
SDSS J185234.98 − 001842.4	V1724 Aql
SDSS J200130.23 + 184255.6	
SDSS J200214.34 + 313634.7	ASASSN-17eo
SDSS J200504.93 + 322122.5	V550 Cyg
SDSS J201222.34 + 325927.5	
SDSS J201649.48 + 382109.3	V1377 Cyg

This paper has been typeset from a TeX/LaTeX file prepared by the author.